CHAPTER 11

Method of Moments

The method of moments (MoM) is a versatile computational method. It can be used to solve differential equations, integral equations, and integro-differential equations. Its use in electromagnetics was pioneered by Harrington [1]. The origin and development of the MoM is very well documented by him [2]. One of the main advantages of this technique lies in its variational nature of the solution, which implies that even if the unknown function (e.g., potential/charge/current) is modeled to first order accuracy, the solution is accurate to the second order [1, p. 18]. The MoM involves a good amount of preprocessing of Maxwell's equations because it makes use of the Green's function. However, the use of Green's function helps solve open region problems such as radiation, scattering, planar circuits, and antennas in an efficient manner. Unlike in other computational methods, the device domain is not discretized, and only the unknown function is discretized in MoM. As a result, this method does not suffer from numerical dispersion and the matrix size is smaller. The limitation of MoM is that this method is generally applied to structures with dimensions of the order of λ. This limitation arises from the computer resources requirements.

11.1 Introduction

The MoM is based on the weighted residual method, which was introduced in Chapter 9, through the solution of differential equation. Here we shall describe the weighted residual method in terms of operator equation, which is symbolic of both the integral and differential equations. We shall first apply the MoM to solve the differential equations with the emphasis on the mathematical concepts and without getting into the physics of the problem. Once these concepts are mastered, the method will be applied to the solution of integral equations.

A general linear, inhomogeneous equation may be described in operator form as

$$L(f) = g \tag{11.1}$$

where L is a linear operator which could be a differential, integral, or integro-differential operator; the function g is known and the corresponding solution f is to be determined. In physical problems, L represents the system, and g the excitation of the system. The unknown function f is expanded in a series of known functions

with unknown amplitudes. The amplitudes are determined using a set of *test* functions. The residual corresponding to (11.1) may be defined as

$$R = L(f) - g \tag{11.2}$$

11.1.1 MoM Procedure

The first step in the solution based on MoM is to choose a set of linearly independent basis/expansion functions $f_1, f_2, f_3, \ldots f_m, \ldots$, in the domain of L, and express the unknown function f in the form of a series; that is,

$$f = \sum_n \alpha_n f_n \tag{11.3}$$

where the complex constants α_n are unknown, and are to be determined. This step is called discretization of function f. The basis functions determine the efficiency of MoM. A poor choice may lead to a divergent solution [3]. The basis functions employed may be of entire domain or subdomain type, and these are discussed in Chapter 6.

In the next step we substitute the expansion (11.3) in (11.2). Using the linearity property of L, we can write

$$R = \sum_n \alpha_n L(f_n) - g \tag{11.4}$$

Expression (11.4) is a single equation with a number of unknowns α_n, which can be determined *uniquely* only if we generate sufficient number of simultaneous equations. For this, we choose a set of test functions $w_1, w_2, w_3, \ldots w_m, \ldots$ in the domain of L, and take the inner product of (11.4) with each of w_m. The inner product between two real functions $\Psi(x)$ and $\Phi(x)$ is defined as

$$<\Psi, \Phi> = \int \Psi(x)\Phi(x)\, dx \tag{11.5}$$

The inner product is also called the moment and therefore the name Method of Moments. Physically, (11.5) denotes projecting function Ψ over the function Φ, as explained in Chapter 6. Taking the inner product of residual with weight functions and setting it to zero results in

$$<R, w_m> = 0 \qquad m = 1, 2, 3, \ldots$$

or in expanded form

$$\sum_n \alpha_n <w_m, L(f_n)> = <w_m, g> \qquad m = 1, 2, 3, \ldots \tag{11.6}$$

The set of simultaneous equations represented by (11.6) *are independent only if the test functions are linearly independent*. The above set of equations can be written in the matrix form as

$$[l][\alpha] = [p] \tag{11.7}$$

where

$$[l] = \begin{bmatrix} <w_1, Lf_1> & <w_1, Lf_2> & \cdots \\ <w_2, Lf_1> & <w_2, Lf_2> & \cdots \\ \cdots & \cdots & \cdots \end{bmatrix} \tag{11.8a}$$

$$[\alpha] = \begin{bmatrix} \alpha_1 \\ \alpha_2 \\ \cdot \\ \cdot \end{bmatrix} \tag{11.8b}$$

$$[p] = \begin{bmatrix} <w_1, g> \\ <w_2, g> \\ \cdot \\ \cdot \end{bmatrix} \tag{11.8c}$$

Next, the matrix equation (11.7) is solved for the vector $[\alpha]$ by using any of the matrix solution techniques described in Appendix A. Finally, the coefficients α_n are substituted in (11.3) to determine f as

$$f = [f]^t[\alpha] \tag{11.9}$$

where

$$[f]^t = [f_1 \quad f_2 \quad \cdots \quad \cdots] \tag{11.10}$$

is the basis vector.

Remarks. The solution based on the MoM could be an exact solution if the basis set, and the test function set is a complete set. However, it may require an infinite number of functions, and a finite number of functions are used in practice because of the finite memory size of the computer. Therefore, the MoM solution is an approximate solution. *The accuracy and numerical efficiency of the MoM depends on our ingenuity in choosing the appropriate set of basis and test functions*. This point will be illustrated further as we work out some problems.

Considerations for the Choice of Basis Functions

1. Since the solution f satisfies the boundary conditions, the basis functions selected must also satisfy the boundary conditions of the problem if we are solving a differential equation. For integral equation solution, the boundary conditions are built into the integral equation and are therefore not imposed on the basis functions.

2. Since (11.3) is substituted in (11.1) to determine α_n, the basis functions should have continuous derivatives if operator L involves differentiation. If the analysis is carried out in the Fourier domain, the basis functions should be Fourier transformable.
3. The basis functions determine the complexity of the integrals for the matrix elements. These integrals can be determined analytically only if simple basis functions are used.

Various types of basis functions are discussed in Chapter 6.

The considerations for the choice of test functions are discussed next. In this context we shall revisit two popular forms of weighted residual method.

11.1.2 Point Matching and Galerkin's Methods

In general, one can choose any set of test functions in the range of operator L. However, it has been observed that some particular choices of test functions are more popular than others. If Dirac delta functions $\delta(.)$ are used as test functions—that is,

$$w_m = \delta(\mathbf{r} - \mathbf{r_m}) \tag{11.11}$$

the resulting integration for the inner product in (11.6) are avoided and merely becomes a substitution. This choice of test function is called *point matching* or *collocation* because the testing in this sense implies satisfying (11.6) at the test point $\mathbf{r_m}$. Point matching MoM process is a useful simplification. At points other than the match points, (11.6) may not be satisfied. Indeed, it has been found to be so. In between these points one can only hope that the operator equation is not so badly violated that the solution becomes useless and may be called spurious solution. The accuracy of the solution improves as the number of match points is increased.

Remarks. It may be pointed out that the use of pulse expansion and point matching in MoM solution is equivalent to using the finite difference method [1, p. 153].

In the Galerkin's method, the test function set is taken identical with the basis function set; that is,

$$w_m = f_m \tag{11.12}$$

An advantage of this method is that we do not have to search for test functions once basis functions have been decided. The Galerkin's method is one of the popular choices.

The requirement that the matrix elements should be finite may rule out certain combinations of testing and basis functions. Also, smoothness of the basis/testing functions affects the convergence and accuracy of the numerical solution. The impact of the choice of test functions on the accuracy of numerical solution has been evaluated for specific problems. For *TM* scattering of plane waves by perfectly

conducting cylinders, the accuracy is determined by the order of the basis functions and not the test functions [2, Section 5.6].

The inhomogeneous equation of (11.1) contains an excitation term on the right side and the operator part on the left side. The operator describes the system properties in terms of natural modes of the system. The excitation function selects the particular mode (modes) of the system. It is important to study the natural modes for complete information about the system. We next study the natural modes of the operator $-d^2/dx^2$ using MoM with emphasis on the convergence behavior. This study is also called the eigenvalue analysis.

11.1.3 Eigenvalue Analysis Using MoM

Let us consider a simple eigenvalue problem described by

$$-\frac{d^2 f}{dx^2} = \lambda f \qquad 0 \le x \le 1 \tag{11.13}$$

subject to the boundary conditions $f(0) = f(1) = 0$. The above eigenvalue equation may represent the natural modes of vibration of a stretched string fixed at the two ends or a line resonator shorted at the ends. The analytical expressions for the eigenvalues and eigenfunctions are: $\lambda_i = (i\pi)^2$ and $f_i(x) = \sqrt{2}\sin(i\pi x)$, $i = 1, 2, 3, \ldots$

Solution. Let us attempt a power series solution by choosing the following basis functions:

$$f_n = x - x^{n+1} \qquad n = 1, 2, 3, \ldots N \tag{11.14}$$

Implementing the Galerkin's approach produces the following matrix equation:

$$[l][\alpha] = \lambda[p][\alpha] \tag{11.15}$$

with the matrix elements given by

$$l_{mn} = \int_0^1 (x - x^{m+1})\, n(n+1)(x^{n-1})\, dx = \frac{mn}{m+n+1} \tag{11.16a}$$

$$p_{mn} = \int_0^1 (x - x^{m+1})(x - x^{n+1})\, dx = \frac{mn(m+n+6)}{3(m+3)(n+3)(m+n+3)} \tag{11.16b}$$

To illustrate the convergence of the numerical solution, let us consider the approximate solutions as the number of basis functions N is increased. For $N = 1$, the matrix element is: $l_{11} = 1/3$ and $p_{11} = 1/30$, and (11.15) gives in this case

$$\frac{1}{3}\alpha_1 = \lambda \frac{1}{30}\alpha_1 \tag{11.17}$$

Hence our first approximation to λ_1 is $\lambda_1^{(1)} = 10$. The superscript here denotes the value of N. The approximate solution compares well with the exact eigenvalue $\lambda_1 = \pi^2 = 9.8696$. The approximate eigenfunction is given by

$$f_1^{(1)}(x) = \alpha_1(x - x^2) \tag{11.18}$$

To compare it with the exact normalized eigenfunction $f_1(x) = \sqrt{2}\sin(\pi x)$, we normalize $f_1^{(1)}$ according to

$$\int_0^1 f_1^{(1)}(x) f_1^{(1)}(x)\, dx = 1 \Rightarrow \alpha_1 = \sqrt{30}$$

and

$$f_1^{(1)}(x) = \sqrt{30}(x - x^2) \tag{11.19}$$

Comparison of this eigenfunction with the exact value $f_1(x) = \sqrt{2}\sin(\pi x)$ shows very little difference over the entire range of x.

Let us now increase the number of basis functions to $N = 2$. Equation (11.15) now becomes

$$\begin{bmatrix} 1/3 & 1/2 \\ 1/2 & 4/5 \end{bmatrix} \begin{bmatrix} \alpha_1 \\ \alpha_2 \end{bmatrix} = \lambda \begin{bmatrix} 1/30 & 1/20 \\ 1/20 & 8/105 \end{bmatrix} \begin{bmatrix} \alpha_1 \\ \alpha_2 \end{bmatrix} \tag{11.20}$$

The eigenvalues found from the determinant are: $\lambda_1^{(2)} = 10$, $\lambda_2^{(2)} = 42$. To obtain the eigenfunctions corresponding to these values of λ, we first substitute the value of $\lambda_1^{(2)}$ in (11.20) and determine α_1 from normalization; this results in

$$f_1^{(2)}(x) = \sqrt{30}(x - x^2) = f_1^{(1)}(x) \tag{11.21}$$

Similarly, the eigenfunction corresponding to $\lambda_2^{(2)} = 42$ is obtained as

$$f_2^{(2)}(x) = 3\sqrt{210}(x - x^2) - 2\sqrt{210}(x - x^3) \tag{11.22}$$

Comparison of this eigenfunction with the exact value $f_2(x) = \sqrt{2}\sin(2\pi x)$ is plotted in Figure 11.1. The agreement for the most part of x appears to be good. Table 11.1 compares the approximate eigenvalues obtained from MoM against the exact analytical solution. It may be noted from this table that the computed eigenvalues $\lambda_i^{(N)}$ are larger than the exact value λ_i for all values of N. This is the property of self-adjoint and positive definite operators like $-d^2/dx^2$ [1]. Also, the

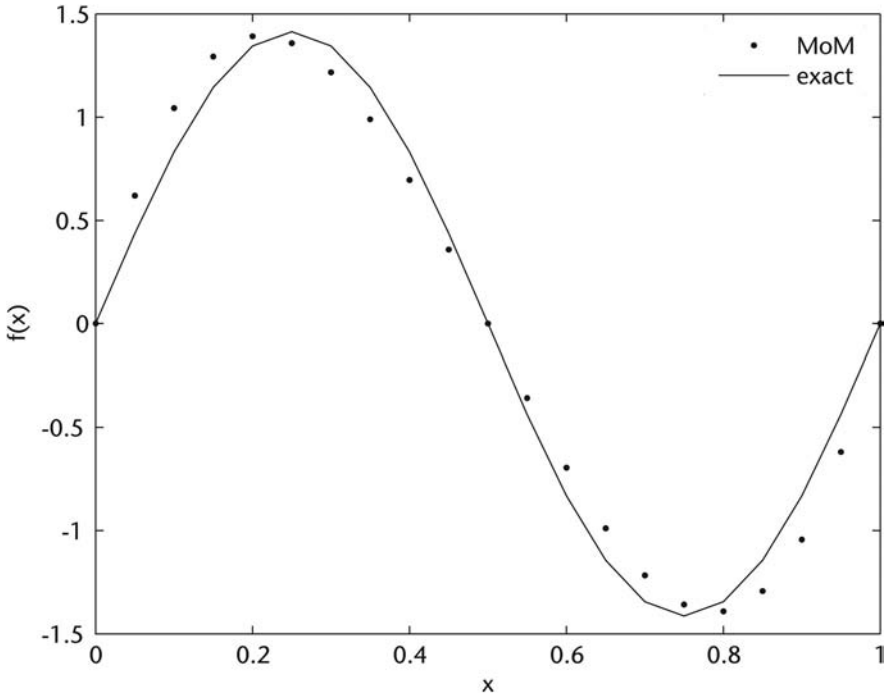

Figure 11.1 Comparison of the MoM solution for $N = 2$ with the exact solution.

Table 11.1 Comparison of Approximate Eigenvalues Based on MoM and Exact Analytical Solution

N	$\lambda_1^{(N)}$	$\lambda_2^{(N)}$	$\lambda_3^{(N)}$	$\lambda_4^{(N)}$
1	10.0000	—	—	—
2	10.0000	42.000	—	—
3	9.8697	42.000	102.133	—
4	9.8697	39.497	102.133	200.583
Exact	9.8696	39.478	88.826	157.914

eigenvalues converge to the exact analytical value as the number of basis functions is increased.

Quiz 11.1. The following (entire domain or subdomain) basis functions are suggested for expanding the unknown function $f(x)$ for the differential equation $-\dfrac{d^2f}{dx^2} = 1 + x^2$ subject to $f(0) = f(1) = 0$. Choose the correct basis functions with justification.

1. $f_n(x) = x - x^n$, $n = 1, 2, 3, \ldots$
2. $f_n(x) = \sin(n\pi x)$, $n = 1, 2, 3, \ldots$
3. Pulse functions $P(x - x_n)$, $n = 1, 2, 3, \ldots$
4. Triangular functions $T(x - x_n)$, $n = 1, 2, 3, \ldots$

Answer. (1) and (4).

11.2 Solution of Integral Equations Using MoM

The problems in electromagnetics may be formulated as differential equations, or integral equations, or integro-differential equations. The differential equation approach is usually the simpler one and can lead to exact solutions. Integral equation solution usually leads to approximate solutions. The boundary conditions are built into the integral equations rather than imposed through the basis functions. The form of kernel in an integral equation depends on the boundary and interface conditions. We next discuss MoM solution of integral equations.

11.2.1 Integral Equation

An integral equation is one for which the unknown quantity appears under the integral sign. An integral equation of the first kind has the following form:

$$\int I(z')K(z, z')\,dz' = -E(z) \tag{11.23}$$

where $K(z, z')$ is called the kernel and is known, and $I(z')$ is the unknown function to be determined. The excitation $E(z)$ is known. *The integral equation in electromagnetics represents a boundary condition*. The formulation of integral equation requires the knowledge of Green's function, which is called kernel in (11.23). A well-known example of kernel is the free space Green's function expressed as

$$K = \frac{e^{-jkr}}{4\pi r} \tag{11.24}$$

with r being the distance between the observation point (x, y, z) and the source point (x', y', z'), and is given by

$$r = \sqrt{(x - x')^2 + (y - y')^2 + (z - z')^2} \tag{11.25}$$

As an example of Green's function and the integral equation in electrostatics consider the Poisson equation,

$$\nabla^2\varphi(\mathbf{r}) = -\frac{\rho(\mathbf{r})}{\epsilon_0 e_r} \tag{11.26}$$

It has a solution in integral form as

$$\varphi(\mathbf{r}) = \frac{1}{4\pi\epsilon_0\,\epsilon_r} \iiint_{V'} \frac{\rho_v(\mathbf{r}')}{|\mathbf{r} - \mathbf{r}'|}\,dv' \tag{11.27}$$

This expression represents an integral equation if the potential function $\varphi(\mathbf{r})$ is known and we seek the charge density distribution $\rho(\mathbf{r}')$, which produces this

potential distribution. The factor $\frac{1}{4\pi\epsilon_0\,\epsilon_r}\,\frac{1}{|\mathbf{r}-\mathbf{r}'|}$ is called the Green's function. The derivation of Green's function is discussed in Chapter 3.

We now illustrate the MoM solution of integral equations.

Example 11.1. Let us apply the method of moments to obtain the approximate solution for the following integral equation [4]:

$$-\frac{1}{2\pi}\int_{-1}^{1} f(x')\,\ell n|x-x'|\,dx' = \frac{\ell n 2}{2} \tag{11.28}$$

and compare the numerical results with the analytical solution

$$f(x) = \frac{1}{\sqrt{1-x^2}} \tag{11.29}$$

Solution. The given integral equation represents the governing equation for an infinite conducting strip charged to a constant potential if $f(x') = q(x')/\epsilon$. The normalized width of the strip is two units. Let us use pulse expansion functions and point matching in the MoM procedure to determine $f(x)$. The unknown function can be expanded as

$$f(x) = \sum_{n=1}^{N} \alpha_n P_n(x - x_n) \tag{11.30}$$

where α_n are the expansion coefficients and $P_n(.)$ are the pulse functions defined in (6.6). The integral equation (11.28) may therefore be written as

$$\sum_{n=1}^{N} \alpha_n \int_{-1}^{1} P_n(x' - x_n')\,\ell n|x-x'|\,dx' = -\pi\ell n 2 \tag{11.31}$$

Consistent with the use of pulse expansion functions we divide the range of x into N equal subintervals of size $h_x = 2/N$. Each of the subintervals is centered at $x_n(= -1 + h_x(n - 1/2))$. Using (6.6) for the pulse function, we obtain

$$\sum_{n=1}^{N} \alpha_n \int_{x_n - h_x/2}^{x_n + h_x/2} \ell n|x-x'|\,dx' = -\pi\ell n 2 \tag{11.32}$$

Point matching at x_m, $m = 1, 2, 3, \ldots N$, is obtained by setting $x = x_m$ and gives

$$\sum_{n=1}^{N} \alpha_n \int_{x_n - h_x/2}^{x_n + h_x/2} \ell n|x_m - x'|\, dx' = -\pi \ell n 2, \qquad m = 1, 2, 3, \ldots N \tag{11.33}$$

The above set of equations may be written as

$$\sum_{n=1}^{N} \alpha_n S_{mn} = -\pi \ell n 2 \tag{11.34}$$

where

$$\begin{aligned} S_{mn} &= \int_{x_n - h_x/2}^{x_n + h_x/2} \ell n|x_m - x'|\, dx' \\ &= \int_{-h_x/2}^{h_x/2} \ell n|x_m - x_n - x'|\, dx' \end{aligned} \tag{11.35}$$

The integral can be evaluated analytically as

$$-S_{mn} = h_x - \frac{h_x}{2} \ell n \left| (x_m - x_n)^2 - \left(\frac{h_x}{2}\right)^2 \right| - (x_m - x_n)\, \ell n \frac{\left| x_m - x_n + \frac{h_x}{2} \right|}{\left| x_m - x_n - \frac{h_x}{2} \right|} \tag{11.36}$$

Next, we select the center of pulse functions as match points; that is, $x_m = -1 + h_x(m - 1/2)$. Therefore, $x_m - x_n = (m - n)h_x$ and

$$S_{mn} = -h_x \left[1 - \ell n h_x - \frac{1}{2} \ell n \left| (m - n)^2 - \frac{1}{4} \right| \right] + h_x (m - n)\, \ell n \frac{\left| m - n + \frac{1}{2} \right|}{\left| m - n - \frac{1}{2} \right|} \tag{11.37}$$

Also,

$$S_{mm} = h_x \left[-1 + \ell n \left(\frac{h_x}{2} \right) \right] \tag{11.38}$$

Properties of [*S*]: It may be observed from (11.37) and (11.38) that:

1. $S_{nm} = S_{mn}$, that is, the matrix is symmetric.
2. The value of S_{mn} depends on (m-n) and note on the individual values of m and n. Therefore, elements along a given diagonal are equal. Such a matrix is called *toeplitz* matrix. From properties (i) and (ii) it can be concluded that there are only N distinct elements in $[S]$, and all elements can be found from the knowledge of first row or first column.
3. The matrix is diagonally dominant because $|S_{mm}| > |S_{mn}|$, $m \neq n$. Usually, computing the inverse of such a matrix or using any other solution method leads to a very stable process.

The set of simultaneous equations (11.34) may be expressed as a matrix equation

$$[S][\alpha] = -\pi \ell n 2[1] \tag{11.39}$$

where [1] is a column vector with unit entries. The matrix equation (11.39) can be solved using any standard matrix solution technique, and the function $f(x)$ is then given by

$$f(x) = [\alpha]^t [P(x)] \tag{11.40}$$

The results of the numerical analysis are compared with the analytical solution in Figure 11.2 for $N = 5$, 10, and 15 basis functions. The software used is *integral_eqn.m*. It may be noted from this plot that the computed charge distribution $f(x)$ approaches the analytical solution as the number of basis functions is increased.

The integral equation (11.28) has also been analyzed using entire domain basis functions of the type $(x)^n$. However, it has been observed that the computed solutions are accurate for $N \leq 9$ and the error increases for higher values of N. The condition number $k(N)$ of the matrix $[S]$ is found to increase rapidly and the matrix becomes ill-conditioned.

11.2.2 Static Charge Distribution on a Wire

We consider a cylindrical wire of radius a and length ℓ as shown in Figure 11.3(a). We assume $\ell \gg a$, so that the cylinder can be approximated as a filamentary wire and the effect of the end caps of the cylinder can be neglected. Let the cylinder be charged so that its surface is an equipotential surface with $\phi = V_0$. For the field point on the surface of the wire where $\phi = V_0$, the integral equation satisfying this boundary condition is obtained from (11.27) and is given by

$$V_0 = \frac{1}{4\pi\epsilon_0} \iint_{S'} \frac{\rho_s(\mathbf{r}')}{R} \, ds' \tag{11.41}$$

for all points on the surface of the wire described by $\rho = a$, $-\ell/2 \leq z \leq \ell/2$, $0 \leq \varphi \leq 2\pi$ for the field points, and $\rho' = a$, $-\ell/2 \leq z' \leq \ell/2$, $0 \leq \varphi' \leq 2\pi$ for the

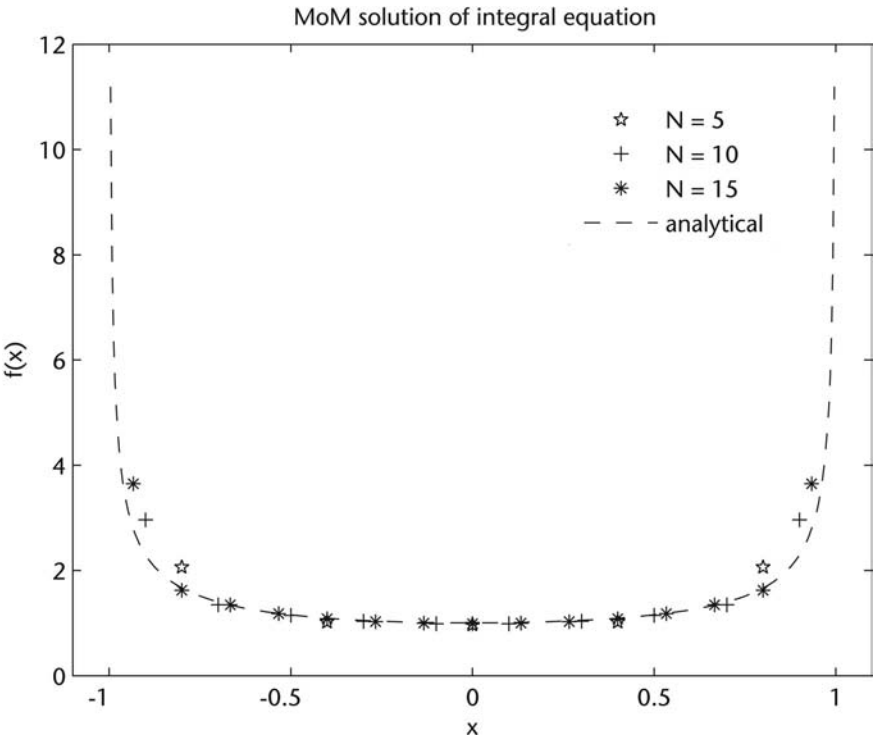

Figure 11.2 Comparison of analytical solution of the integral equation with MoM solution for pulse basis and point matching.

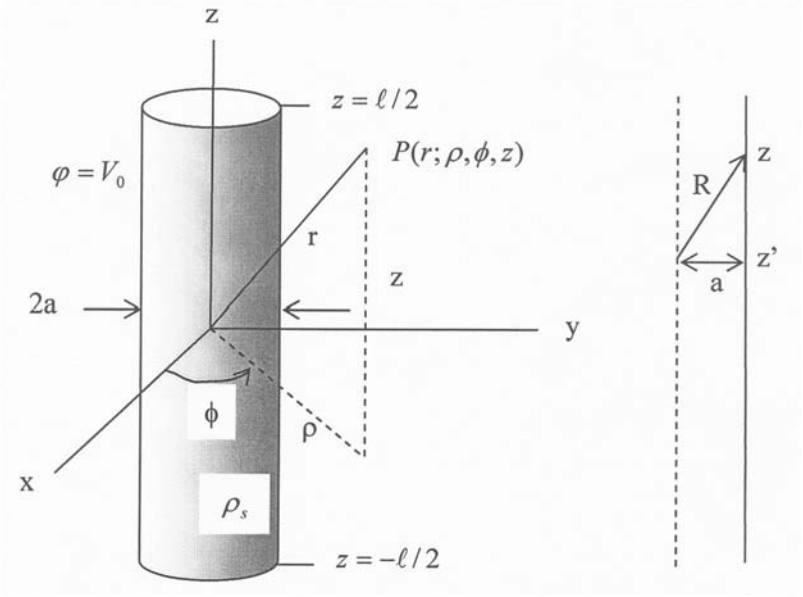

Figure 11.3 (a) A charged conducting wire of radius a and length l with an unknown surface charge density. (b) Simplified model to calculate the distance between the source point and field point. The source point is assumed located at $\rho' = 0$.

source points. Because of the axial symmetry of the wire, we expect the charge density ρ_s to vary with z' and not with φ'. Equation (11.41) can therefore be written as ($ds' = ad\varphi'\, dz'$)

$$V_0 = \frac{1}{4\pi\epsilon_0} \int_{-\ell/2}^{\ell/2} \rho_s(z') \int_0^{2\pi} \frac{1}{R}\, ad\varphi'\, dz' \tag{11.42}$$

where

$$R = |\mathbf{r} - \mathbf{r}'| = \sqrt{2a^2 - 2a^2 \cos\,\varphi' + (z - z')^2} = \sqrt{4a^2 \sin^2\left(\frac{\varphi'}{2}\right) + (z - z')^2} \tag{11.43}$$

We have chosen $\varphi = 0$ for convenience, because the potential is independent of φ. Assuming that the wire radius a is small, it can be shown that the integration over φ' can be approximated as [3]

$$\int_0^{2\pi} \left[4a^2 \sin^2\left(\frac{\varphi'}{2}\right) + (z - z')^2\right]^{-1/2} d\varphi' \cong 2\pi[a^2 + (z - z')^2]^{-1/2} \tag{11.44}$$

The above approximation amounts to assuming that the potential at $\rho = a$ arises from the line charge assumed located at $\rho = 0$ so that $R = \sqrt{a^2 + (z - z')^2}$. The simplified model is shown in Figure 11.3(b). This approximation also removes the singularity in the Green's function at $r = r'$. Use of (11.44) in (11.42) gives

$$V_0 = \frac{a}{2\epsilon_0} \int_{-\ell/2}^{\ell/2} \frac{\rho_s(z')\, dz'}{\sqrt{a^2 + (z - z')^2}} \qquad \text{for } -\frac{\ell}{2} \le z \le \frac{\ell}{2} \tag{11.45}$$

The integral equation is to be solved for the unknown charge density $\rho_s(z')$. As a first step, we expand $\rho_s(z')$ into a sum of N linearly independent basis functions,

$$\rho_s(z') = \sum_{n=1}^{N} \alpha_n f_n(z') \tag{11.46}$$

Substituting in (11.45) gives

$$V_0 = \frac{a}{2\epsilon_0} \int_{-\ell/2}^{\ell/2} \sum_{n=1}^{N} \alpha_n \frac{f_n(z')\, dz'}{\sqrt{a^2 + (z - z')^2}} \qquad \text{for } -\frac{\ell}{2} \le z \le \frac{\ell}{2} \tag{11.47}$$

Because the integral operator is linear, we can interchange the order of summation and integration, and obtain

$$\frac{2\epsilon_0 V_0}{a} = \sum_{n=1}^{N} \alpha_n \int_{-\ell/2}^{\ell/2} \frac{f_n(z')\,dz'}{\sqrt{a^2 + (z - z')^2}} \qquad \text{for } -\frac{\ell}{2} \le z \le \frac{\ell}{2} \tag{11.48}$$

To simplify numerical calculations we use point matching, and implement it by setting $z = z_m$ at the test points. The test points are taken as equi-spaced points on the wire and are defined as

$$z_m = \frac{\left(m - \frac{1}{2}\right)\ell}{N} - \frac{\ell}{2} \qquad m = 1, 2, \ldots, N \tag{11.49}$$

After point matching, the integral equation takes the following form:

$$\frac{2\epsilon_0 V_0}{a} = \sum_{n=1}^{N} \alpha_n \int_{-\ell/2}^{\ell/2} \frac{f_n(z')\,dz'}{\sqrt{a^2 + (z_m - z')^2}} \qquad m = 1, 2, \ldots N \tag{11.50}$$

Let us denote for conciseness

$$I_{mn} = \frac{a}{2\epsilon_0 V_0} \int_{-\ell/2}^{\ell/2} \frac{f_n(z')\,dz'}{\sqrt{a^2 + (z_m - z')^2}} \tag{11.51}$$

Equation (11.50) thus can be written as

$$1 = \sum_{n=1}^{N} \alpha_n I_{mn} \qquad m = 1, 2, \ldots N \tag{11.52}$$

The set of simultaneous equations may be expressed in matrix form as

$$\begin{bmatrix} 1 \\ 1 \\ 1 \\ \vdots \\ 1 \end{bmatrix} = \begin{bmatrix} I_{11} & I_{12} & I_{13} & \ldots & I_{1N} \\ I_{21} & I_{22} & I_{23} & \ldots & I_{2N} \\ I_{31} & I_{32} & I_{33} & \ldots & I_{3N} \\ \vdots & \vdots & \vdots & \vdots & \vdots \\ I_{N1} & I_{N2} & I_{N3} & \ldots & I_{NN} \end{bmatrix} \begin{bmatrix} \alpha_1 \\ \alpha_2 \\ \alpha_3 \\ \vdots \\ \alpha_N \end{bmatrix}$$

or

$$[1] = [I][\alpha] \tag{11.53}$$

The matrix equation can be solved for the vector $[\alpha]$ using any standard matrix solution technique (see Appendix A).

Evaluation of Matrix Elements. The evaluation of matrix elements in the MoM solution in general consumes a large amount of processor time. Therefore, it is desirable to reduce this computer time through analytical simplification of the integrals. For this we consider the integral

$$I = \int_{-\ell/2}^{\ell/2} \frac{f_n(z')\,dz'}{\sqrt{a^2 + (z_m - z')^2}} \tag{11.54}$$

It is important to evaluate the integral near $z' = z_m$ more accurately because of near singularity conditions. When $z' = z_m$, the denominator is very small because the radius a is assumed to be small. The integrand, therefore, becomes highly peaked and requires more sampling points (of the order of a few hundred) for accurate evaluation. In order to correct this condition analytically, we use singularity subtraction method of Appendix B and express the integral as

$$I = \int_{-\ell/2}^{\ell/2} \frac{f_n(z') - f_n(z_m) + f_n(z_m)}{\sqrt{a^2 + (z_m - z')^2}}\,dz'$$

or

$$I = f_n(z_m) \int_{-\ell/2}^{\ell/2} \frac{dz'}{\sqrt{a^2 + (z_m - z')^2}} + \int_{-\ell/2}^{\ell/2} \frac{f_n(z') - f_n(z_m)}{\sqrt{a^2 + (z_m - z')^2}}\,dz' \tag{11.55}$$

The first integral can be determined analytically to give

$$I = f_n(z_m) \ln \frac{z_m + \frac{\ell}{2} + \sqrt{a^2 + \left(z_m + \frac{\ell}{2}\right)^2}}{z_m - \frac{\ell}{2} + \sqrt{a^2 + \left(z_m - \frac{\ell}{2}\right)^2}} + \int_{-\ell/2}^{\ell/2} \frac{f_n(z') - f_n(z_m)}{\sqrt{a^2 + (z_m - z')^2}}\,dz' \tag{11.56}$$

The integrand is zero at $z' = z_m$ and is smooth elsewhere, and can therefore be evaluated numerically.

Use of Entire Domain Basis Functions

In order to determine the matrix elements of (11.56), we need to decide about the expansion functions $f_s(z)$, the choice of which is critical for the efficiency of MoM solution process. The nature of $\rho_s(z')$ is such that we expect it to be symmetric about $z' = 0$, largest near the wire ends due to the Coulomb forces of repulsion, and smallest in the middle of the wire. The entire domain basis functions in the form of simple power series expansion and satisfying the above conditions may be written as

$$f_n(z') = \left(\frac{z'}{\ell/2}\right)^n \qquad \text{for } -\frac{\ell}{2} \le z' \le \frac{\ell}{2} \tag{11.57}$$

The charge density may therefore be expressed as

$$\rho_s(z') = \sum_{n=0}^{N} \alpha_n \left(\frac{2z'}{\ell}\right)^n \tag{11.58}$$

Computed results for this choice of expansion functions for ℓ = 2m, $a = 10^{-2}$ m, equally spaced matching points z_m with N = 6, 12, and 20 and $2\epsilon_0 V_0/a = 1$ are shown in Figure 11.4. The software used is *charge_density_wire1.m*. It may be noted from this figure that the use of higher order expansion functions corresponding to N = 20 produces the edge singularity better and should therefore lead to a more accurate solution. Also, the edge singularity in charge is described analytically by $1/\sqrt{(\ell/2)^2 - z^2}$.

Use of Subdomain Basis Functions

The use of subdomain basis functions like pulse or linear type makes the evaluation of matrix elements simpler. Let us use pulse expansion functions to model the charge density as,

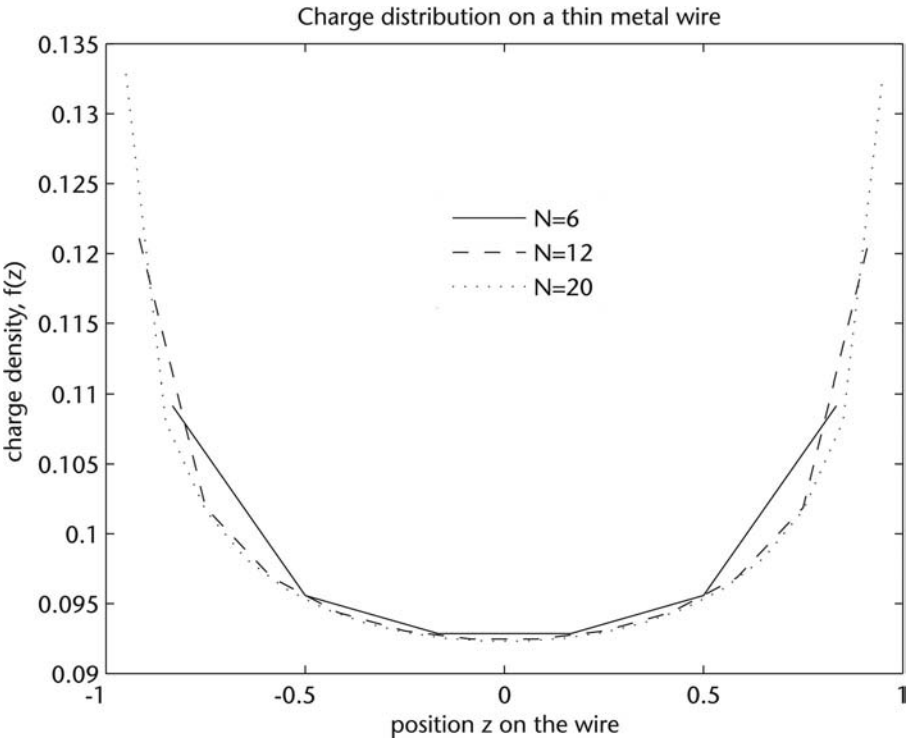

Figure 11.4 Approximate charge density on a conducting wire with length ℓ = 2m, radius a = 1 cm, MoM solution using entire domain expansion functions and point matching.

$$\rho_s(z') = \sum_{n=1}^{N} \alpha_n P_n(z' - z_n) \tag{11.59}$$

where the pulse function has been defined in (6.6). Since $P_n(z' - z_n)$ is constant over each pulse, the integral in (11.54) reduces to [5]

$$I = \int_{z_n - h_z/2}^{z_n + h_z/2} \frac{dz'}{\sqrt{a^2 + (z_m - z')^2}}, \qquad h_z = \frac{\ell}{2N} \tag{11.60}$$

or

$$I = \ln \frac{z_m - z_n + \frac{h_z}{2} + \sqrt{a^2 + \left(z_m - z_n + \frac{h_z}{2}\right)^2}}{z_m - z_n - \frac{h_z}{2} + \sqrt{a^2 + \left(z_m - z_n - \frac{h_z}{2}\right)^2}} \tag{11.61}$$

or

$$I = 2 \ln \frac{\frac{h_z}{2} + \sqrt{a^2 + \left(\frac{h_z}{2}\right)^2}}{a} \qquad \text{for } m = n \tag{11.62a}$$

$$I = \ln \frac{z_m - z_n + \frac{h_z}{2} + \sqrt{a^2 + \left(z_m - z_n + \frac{h_z}{2}\right)^2}}{z_m - z_n - \frac{h_z}{2} + \sqrt{a^2 + \left(z_m - z_n - \frac{h_z}{2}\right)^2}} \qquad \text{for } m \neq n,\ |m - n| \leq 2 \tag{11.62b}$$

$$I = \ln \frac{z_m - z_n + \frac{h_z}{2}}{z_m - z_n - \frac{h_z}{2}} \qquad \text{for } |m - n| > 2 \tag{11.62c}$$

The results for pulse expansion functions is shown in Figure 11.5 for $N = 20$ pulses for equi-spaced test points. The software used is *charge_density_wire2.m*.

Comparison of Solutions Based on Entire Domain and Subdomain Basis

The matrix $[l]$ for these basis functions behaves very differently: (1) the matrix for the pulse basis is symmetric, whereas it is asymmetric for the entire basis; (2) the matrix is diagonally dominant for the pulse basis and not for entire domain basis; (3) the condition number of the matrix $k(N)$ increases with N, slowly for pulse basis and very rapidly for entire basis (e.g., $k(5) = 64$, $k(10) = 1.743 \times 10^4$, and $k(15) = 5.427 \times 10^6$ for the entire domain basis, and $k \approx 3$ for pulse basis). However, the accuracy of the solution is similar for the two types of basis functions.

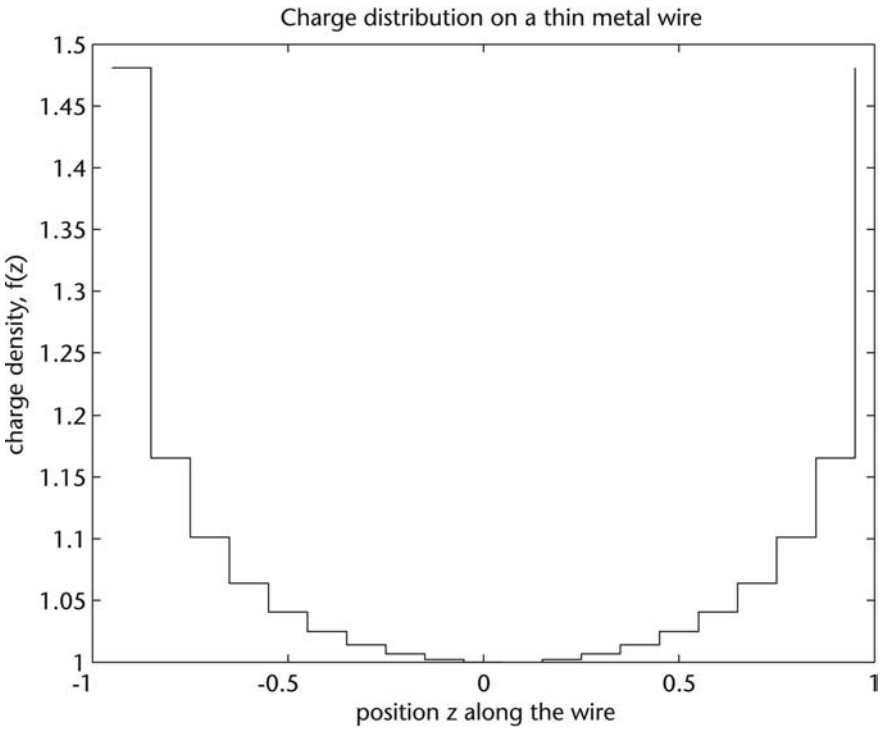

Figure 11.5 Charge density distribution on a wire of length ℓ = 2m, radius a = 1 cm, pulse basis functions and point testing. Number of basis functions, N = 20.

Remarks. The MoM solution presented for a charged wire shows the usefulness of this procedure to determine the unknown charge density, which may be used to calculate the capacitance. The calculation of diagonal elements of the matrix is a sticky point in MoM because of the singularity of the integrand. Next we present a two-dimensional case study.

11.2.3 Analysis of Strip Line

Let us determine capacitance per unit length C_0 of a strip line. This example has been chosen because the Green's function for strip line can be expressed in closed form, and the integration for the matrix elements can be carried out analytically. Figure 11.6 shows the cross-section of a strip line with strip width W and ground

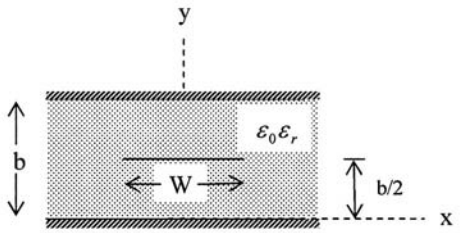

Figure 11.6 Cross-section of a strip line geometry.

planes separation b. For the TEM mode of propagation in strip line, the potential $\varphi(x, y)$ satisfies the Poisson equation

$$\nabla_t^2 \varphi(x, y) = -\frac{\rho(x, y)}{\epsilon} \tag{11.63}$$

and the following boundary conditions:

$$\varphi = 0 \text{ at } y = 0, b \tag{11.64a}$$

$$\varphi = 0 \text{ at } x = \pm\infty \tag{11.64b}$$

$$\varphi = V_0 \text{ at the strip} \tag{11.64c}$$

Here, $\rho(x, y)$ is the charge density on the strip.

The solution of (11.63) may be obtained using the Green's function and the superposition theorem as (see Chapter 3)

$$\varphi(x, y) = \iint G(x, y; x', y')\, \rho(x', y')\, dx'\, dy' \tag{11.65}$$

where $G(x, y; x', y')$ is the Green's function for the problem and is defined as

$$\nabla_t^2 G(x, y; x', y') = -\frac{\delta(x - x')\, \delta(y - y')}{\epsilon} \tag{11.66}$$

subject to

$$G = 0 \text{ at } y = 0, b \tag{11.67a}$$

$$G = 0 \text{ at } x = \pm\infty \tag{11.67b}$$

The integral equation for the strip line problem is obtained by employing the boundary condition $\varphi(x, y) = V_0$ on the strip (at $y = b/2$); that is,

$$V_0 = \iint\limits_{strip} G\left(x, \frac{b}{2}; x', y'\right) \rho(x', y')\, dx'\, dy' \text{ for } -\frac{w}{2} \le x \le \frac{w}{2} \tag{11.68}$$

The Green's function for the strip line is found to be (Problem 3.15)

$$G(x, y; x', y') = \frac{1}{\pi \epsilon_0 \epsilon_r} \sum_{n=1}^{\infty} \frac{1}{n} \sin\left(\frac{n\pi y}{b}\right) \sin\left(\frac{n\pi y'}{b}\right) e^{-n\pi |x - x'|/b} \tag{11.69}$$

To Determine $\rho(x', y')$ on the Strip. For an infinitely thin strip (strip metal thickness $\to 0$), we can express $\rho(x', y') = \rho(x')\,\delta(y' - b/2)$. Further assuming $V_0 = 1$ volt, the integral equation (11.68) reduces to

$$1 = \int_{-W/2}^{W/2} G\left(x, \frac{b}{2}; x', \frac{b}{2}\right) \rho(x')\, dx'$$

$$= \frac{1}{\pi\epsilon_0 \epsilon_r} \sum_{n=1}^{\infty} \frac{1}{n} \sin\left(\frac{n\pi}{2}\right) \sin\left(\frac{n\pi}{2}\right) \int_{-W/2}^{W/2} e^{-n\pi|x-x'|/b} \rho(x')\, dx'$$

or

$$1 = \frac{1}{\pi\epsilon_0 \epsilon_r} \sum_{n,\,odd}^{\infty} \frac{1}{n} \int_{-W/2}^{W/2} e^{-n\pi|x-x'|/b} \rho(x')\, dx' \tag{11.70}$$

Let us expand the unknown charge distribution $\rho(x')$ as

$$\rho(x') \approx \sum_{m=1}^{M} \alpha_m f_m(x') \tag{11.71}$$

Substitute this expansion in (11.70) to obtain

$$1 \approx \frac{1}{\pi\epsilon_0 \epsilon_r} \sum_{n,\,odd}^{\infty} \frac{1}{n} \int_{-W/2}^{W/2} e^{-n\pi|x-x'|/b} \sum_{m=1}^{M} \alpha_m f_m(x')\, dx' \tag{11.72}$$

We shall use subdomain expansion functions. Therefore, we divide the strip into M segments each of length $h_x = w/M$. The mth segment or cell is denoted by Δx_m with the center at x_m according to

$$x_m = -\frac{w}{2} + h_x\left(m - \frac{1}{2}\right) \qquad m = 1, 2, 3, \ldots M \tag{11.73a}$$

and

$$x_m - \frac{h_x}{2} \le \Delta x_m \le x_m + \frac{h_x}{2} \tag{11.73b}$$

MoM Solution Using Pulse Expansion and Point Matching. Using the property of the pulse functions $P(x' - x_m)$ that they have unit amplitude and are nonzero only over the length of the segment $\Delta x_m = h_x$, (11.72) becomes

$$\frac{1}{\pi\epsilon_0\epsilon_r}\sum_{n,odd}^{\infty}\frac{1}{n}\sum_{m=1}^{M}\alpha_m\int_{\Delta x_m}e^{-n\pi|x-x'|/b}\,dx'\approx 1 \tag{11.74}$$

For point matching, we enforce the condition at the mid-point of the segment, say, at $x = x_p$. Expression (11.74) therefore reduces to

$$\frac{1}{\pi\epsilon_0\epsilon_r}\sum_{n,odd}^{\infty}\frac{1}{n}\sum_{m=1}^{M}\alpha_m\int_{\Delta x_m}e^{-n\pi|x_p-x'|/b}\,dx'\approx 1 \tag{11.75}$$

Let us denote for conciseness

$$I(x_p, x_m)\equiv\frac{1}{\pi\epsilon_0\epsilon_r}\sum_{n,odd}^{\infty}\frac{1}{n}\int_{\Delta x_m}e^{-n\pi|x_p-x'|/b}\,dx' \tag{11.76}$$

The expression (11.75) can then be written as

$$\sum_{m=1}^{M}\alpha_m I(x_p, x_m)\approx 1$$

or

$$\alpha_1 I(x_p, x_1)+\alpha_2 I(x_p, x_2)+\ldots+\alpha_m I(x_p, x_m)+\ldots+\alpha_M I(x_p, x_M)\approx 1 \tag{11.77}$$

This equation implies that at $x = x_p$, the sum of the potentials produced by all the M segments is set equal to unity, the potential at the strip. We enforce (11.77) at all the M points of the strip in order to generate M simultaneous equations as given next:

$$\begin{aligned}
&\text{at } x = x_1 && \alpha_1 I(x_1, x_1)+\alpha_2 I(x_1, x_2)+\alpha_3 I(x_1, x_3)+\ldots+\alpha_M I(x_1, x_M)\approx 1\\
&\text{at } x = x_2 && \alpha_1 I(x_2, x_1)+\alpha_2 I(x_2, x_2)+\alpha_3 I(x_2, x_3)+\ldots+\alpha_M I(x_2, x_M)\approx 1\\
&\text{at } x = x_3 && \alpha_1 I(x_3, x_1)+\alpha_2 I(x_3, x_2)+\alpha_3 I(x_3, x_3)+\ldots+\alpha_M I(x_3, x_M)\approx 1\\
&\vdots && \vdots\\
&\text{at } x = x_M && \alpha_1 I(x_M, x_1)+\alpha_2 I(x_M, x_2)+\alpha_3 I(x_M, x_3)+\ldots+\alpha_M I(x_M, x_M)\approx 1
\end{aligned} \tag{11.78}$$

The above set of equations may be written in matrix form as

$$\begin{bmatrix} I(x_1, x_1) & I(x_1, x_2) & \ldots & I(x_1, x_M)\\ I(x_2, x_1) & I(x_2, x_2) & \ldots & I(x_2, x_M)\\ \vdots & \vdots & \vdots & \vdots\\ I(x_M, x_1) & I(x_M, x_2) & \ldots & I(x_M, x_M)\end{bmatrix}\begin{bmatrix}\alpha_1\\ \alpha_2\\ \vdots\\ \alpha_M\end{bmatrix}=\begin{bmatrix}1\\ 1\\ \vdots\\ 1\end{bmatrix} \tag{11.79}$$

Let us write

$$I_{pm} = I(x_p, x_m) = \frac{1}{\pi\epsilon_0\epsilon_r} \sum_{n,odd}^{\infty} \frac{1}{n} \int_{\Delta x_m} e^{-n\pi|x_p - x'|/b}\, dx' \tag{11.80}$$

Each of the equations of (11.78) can be written as

$$\sum_{m=1}^{M} \alpha_m I_m = 1 \qquad p = 1, 2, 3, \ldots M \tag{11.81}$$

or in matrix form

$$[I][\alpha] = [1] \tag{11.82}$$

where $[\alpha]$ and $[1]$ are column vectors of size M and $[I]$ is an $M \times M$ square matrix. The vector $[\alpha]$ can be determined using any matrix solution technique. Substituting for $[\alpha]$ in (11.71) gives the approximate solution of the integral equation as

$$\rho(x) \approx [\alpha]^t [P] \tag{11.83}$$

where $[\alpha]^t$ is the transpose of vector $[\alpha]$.

Determination of Matrix Elements. The matrix elements I_{pm} may be determined as,

$$I_{pm} = \frac{1}{\pi\epsilon_0\epsilon_r} \sum_{n,odd}^{\infty} \frac{1}{n} \int_{\Delta x_m} e^{-n\pi|x_p - x'|/b}\, dx' \tag{11.84}$$

$$= \frac{1}{\pi\epsilon_0\epsilon_r} \sum_{n,odd}^{\infty} \frac{1}{n} \int_{x_m - h_x/2}^{x_m + h_x/2} e^{-n\pi|x_p - x'|/b}\, dx'$$

with x_m given by (11.73a). Carrying out the integration gives (independent of $x_p > x'$ or $x_p < x'$)

$$I_{pm} = \frac{1}{\pi\epsilon_0\epsilon_r} \frac{2b}{\pi} \sum_{n,odd}^{\infty} \frac{1}{n^2} e^{-n\pi|x_p - x_m|/b} \sinh\left(\frac{n\pi}{2b} h_x\right) \tag{11.85}$$

The charge density distribution on the thin strip with $W/b = 1.5$, and $\epsilon_r = 1$ is plotted in Figure 11.7 for $N = 30$. The software employed is *stripline.m*. The number of terms used in the summation for Green's function (11.69) is also 30. The charge distribution shows the expected edge singularity.

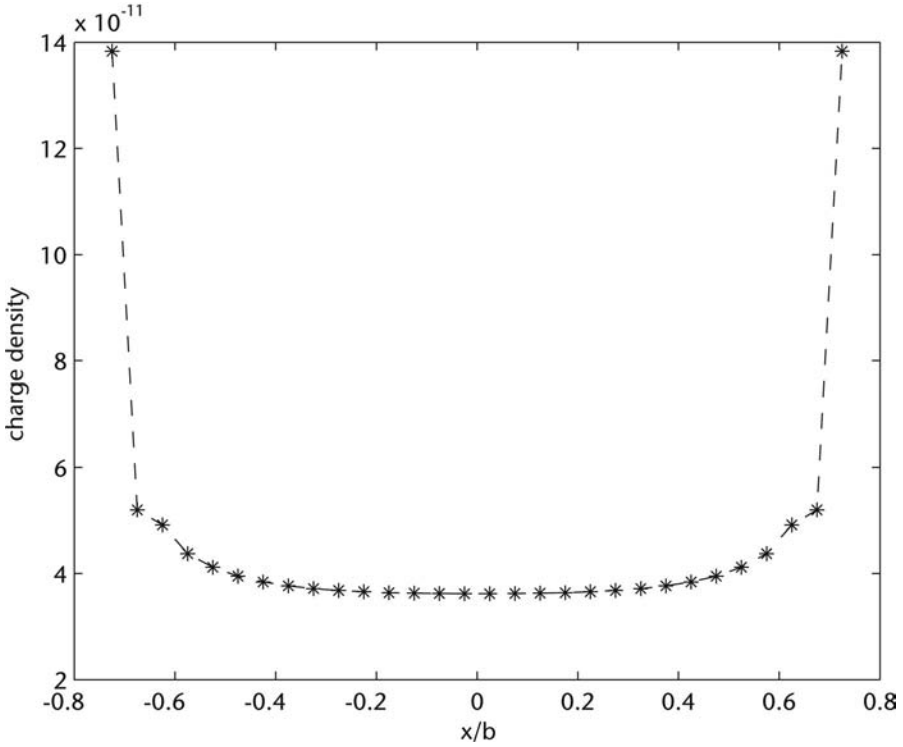

Figure 11.7 Charge density distribution on a strip for $W/b = 1.5$, $\epsilon_r = 1.0$. Pulse expansion and point matching with $N = 30$, the number of terms used in the Green's function is 30.

Determination of C_0. The charge density computed above may be used to determine the capacitance per unit length of strip line. For the assumed $V_0 = 1$ volt, the capacitance per unit length C_0 is given by

$$C_0 = \frac{Q}{V_0} = Q \tag{11.86}$$

where Q is the total charge on the strip and is given by

$$Q = \iint_{strip} \rho(x', y')\, dx'\, dy' = \int_{-W/2}^{W/2} \rho(x')\, dx' \tag{11.87}$$

for zero thickness metal strip. For pulse modeling of the charge,

$$Q = \sum_{n=1}^{N} \alpha_n \int_{h_x} p_n(x)\, dx = \sum_{n=1}^{N} \alpha_n \tag{11.88}$$

The characteristic impedance is given by

$$Z_0 = \frac{1}{C_0 v} \tag{11.89}$$

where v is the phase velocity of the wave in the transmission line. Since the strip line is homogeneously filled, $v = 1/\sqrt{\mu_0 \epsilon_0 \epsilon_r}$. Therefore,

$$Z_0 = \frac{\sqrt{\mu_0 \epsilon_0 \epsilon_r}}{\sum \alpha_n} \tag{11.90}$$

The computed value of characteristic impedance of the strip line for $N = 20$, $W/b = 1.5$ and $\epsilon_r = 1$ is found to be 47.92 ohms. The conformal mapping solution for the strip line (Chapter 4) gives the following closed-form expression:

$$Z_0 = \frac{29.976\pi}{\sqrt{\epsilon_r}} \frac{K(k)}{K'(k)}, \qquad k = \operatorname{sech}\left(\frac{\pi W}{2b}\right), \qquad k' = \tanh\left(\frac{\pi W}{2b}\right) \tag{11.91}$$

The expression for the ratio of elliptic functions is given in (4.117). The characteristic impedance based on (11.91) is found to be 48.2 ohms, and the comparison with the computed value is very good.

Fringing Field Capacitance

The approximate electric field distribution in strip line is shown in Figure 11.8. The field lines between the strip and the ground planes contribute to the parallel plate capacitance C_p; and the fringing electric field at the edges may be described by C_f. The capacitance per unit length C_0 may therefore be divided as

$$C_0 = C_p + 2C_f \tag{11.92}$$

The capacitance C_p is given by

$$C_p = 2\frac{\epsilon_0 \epsilon_r W}{\frac{b}{2}} \tag{11.93}$$

The capacitance C_f can be determined from C_0, C_p, and (11.92). For the example considered above, one finds that C_0 is 69.56 pF/m, C_p is 53.125 pF/m, and therefore $C_f = 8.217$ pF/m.

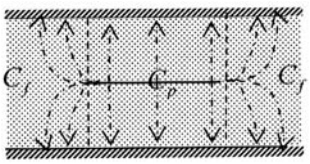

Figure 11.8 Modeling line capacitance C_0 in terms of parallel plate capacitance C_p and fringing field capacitance C_f.

It is seen that C_f, and therefore fringing field, increases with the increase in dielectric thickness b and decrease in the value of dielectric constant ϵ_r of the substrate. This property is useful while selecting the substrate for circuit and antenna applications. Low value of C_f imply lower amount of radiation. Therefore, high value of ϵ_r and thinner substrate is used for circuit applications, and vice versa, for antennas.

Quiz 11.2. The charge density distribution on a metal strip or a thin wire of finite length is marked by singularity at the ends. While simulating this distribution, if the number of test points per unit length is increased from, say, 12 to 24, the distribution will be marked by:

1. Larger edge singularity;
2. Flatter central region;
3. No change in distribution.

Please choose the correct options and explain why.

Answer. (1) and (2).

Quiz 11.3. The integral equation solution based on MoM and pulse basis functions is characterized by:

1. Diagonal matrix elements dominate the matrix
2. Diagonal matrix elements involve pole singularity
3. The matrix is symmetric about the diagonal
4. The matrix is tridiagonal or sparse

Comment on the above and justify the choice.

Answer. (1), (2), and (3) are correct.

11.2.4 Analysis of Wire Dipole Antenna

When the wire of Section 11.2.1 is excited by a time varying electromagnetic field, a current density $\mathbf{J_s}$ (ampere per meter) is induced on the wire surface. The induced current reradiates and produces an electric field called the radiation or scattered field. If the source of excitation is on the wire itself, the wire dipole is called a transmitting antenna. For a distant source, the dipole may act as a receiving antenna if a receiver is connected to it; otherwise it is called a scatterer. The problem of wire antenna may be analyzed using either Pocklington's integral equation or Hallen's integral equation. The presentation for the Pocklington's integral equation here follows [5].

Consider a very thin wire of radius a and length ℓ as shown in Figure 11.9(a). Let us connect an excitation source across the gap so that the wire behaves as a radiating dipole antenna. The integral equation for the antenna may be obtained from the boundary condition that the sum of the radiated field E_z and the excitation field E_z^i must be zero on the surface of a perfectly conducting wire; that is,

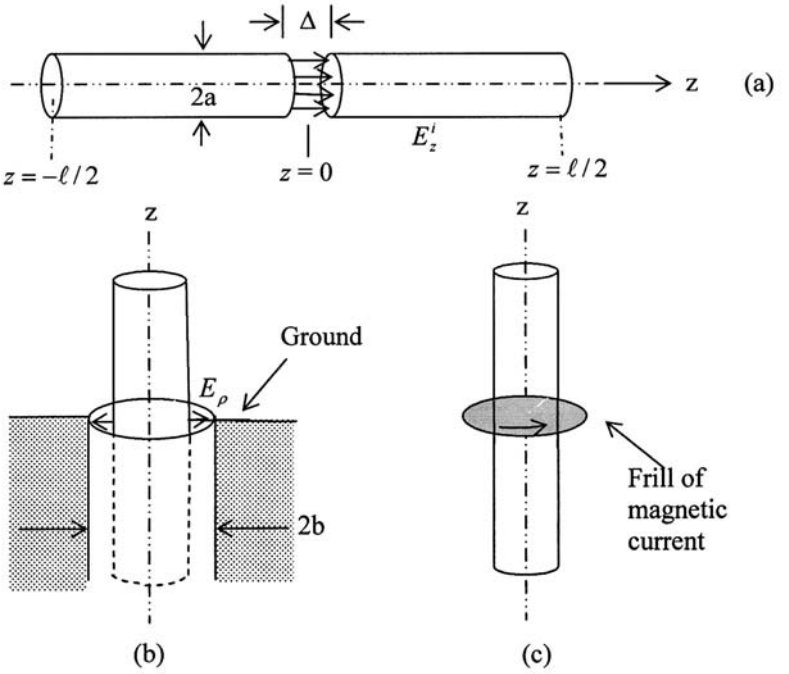

Figure 11.9 Wire antenna and the excitation models: (a) the delta gap model with the impressed electric field; (b) coaxial line feeding a monopole through the ground plane; and (c) wire antenna and magnetic frill generator.

$$E_z = -E_z^i \qquad \text{for } -\frac{\ell}{2} \le z \le \frac{\ell}{2},\ \rho = a,\ 0 \le \varphi \le 2\pi \tag{11.94}$$

For a very thin wire ($a \ll \lambda$), one may neglect the circumferential current and approximate the total current by the longitudinal component J_z. Also, due to the circular symmetry of the wire, J_z is not a function of angle ϕ and can be replaced by a filamentary line source of current $I(z')$ given by

$$I(z') = \int_0^{2\pi} J_z(z')\, a d\phi = 2\pi a J_z(z') \tag{11.95}$$

The electric field produced by this current can be derived from the vector potential **A** using the following expression [see (1.40a)]:

$$j\omega\epsilon_0 \mathbf{E} = \nabla\nabla.\mathbf{A} + k^2\mathbf{A} \tag{11.96}$$

where the vector potential is related to the current density through (1.39),

$$\nabla^2 A_z + k^2 A_z = -\mu J_z \tag{11.97}$$

and k is the free space wavenumber. Once the potential A_z is obtained, the electric field produced by it is given by (11.96),

$$E_z = \frac{1}{j\omega\epsilon_0}\left[\frac{d^2A_z}{dz^2} + k^2A_z\right] \tag{11.98}$$

The potential A_z may be determined by solving (11.97) through the Green's function method (Chapter 3), and is given by

$$A_z = \iint_{s'} J_z G(z; z')\, ds' = \int_{-l/2}^{l/2}\int_{0}^{2\pi} J_z G(z; z')\, a d\phi'\, dz' \tag{11.99}$$

where $G(z; z') = e^{-jkr}/(4\pi r)$ is the free space Green's function. Using (11.95) for J_z gives the following expression:

$$\begin{aligned} A_z &= \frac{1}{2\pi a}\int_{-l/2}^{l/2} dz' \int_{0}^{2\pi} I(z')\frac{e^{-jkr}}{4\pi r}\, a d\phi' \\ &= \frac{1}{2\pi}\int_{-l/2}^{l/2} dz' \int_{0}^{2\pi} I(z')\frac{e^{-jkr}}{4\pi r}\, d\phi' \end{aligned} \tag{11.100}$$

where r is the distance between the source point and the observation point. Since the current at *rf* frequencies is concentrated on the metal surface and the observation point should also be on the surface to satisfy the boundary condition, the expression for r is given by

$$r = \sqrt{2a^2 - 2a^2\cos(\varphi - \phi') + (z - z')^2} \tag{11.101}$$

Simplification of the Integral for A_z

To simplify the evaluation of the integral in (11.100), we choose $\phi = 0$. As a result,

$$r = \sqrt{2a^2 - 2a^2\cos\,\phi' + (z - z')^2} = \sqrt{4a^2\sin^2\left(\frac{\phi'}{2}\right) + (z - z')^2} \tag{11.102}$$

We assume further that the current resides along the axis of the wire as discussed in Section 11.2.1. This assumption simplifies the expression for r to [5]

$$r = \sqrt{a^2 + (z - z')^2} \tag{11.103}$$

and also implies that the contribution of singularity to the integral is not significant for the accuracy considered here.

The expression for r is now independent of ϕ' and (11.100) therefore reduces to

$$A_z = \int_{-l/2}^{l/2} I(z') \frac{e^{-jkr}}{4\pi r}\, dz' = \int_{-l/2}^{l/2} I(z')\, G(z, z')\, dz' \tag{11.104}$$

Use of this expression in (11.98) gives the following expression for the field produced by the induced current:

$$E_z = \frac{1}{j\omega\epsilon_0} \int_{-\ell/2}^{\ell/2} \left[\frac{\partial^2 G(z; z')}{\partial z^2} + k^2 G(z; z') \right] I(z')\, dz' \tag{11.105}$$

where

$$G(z; z') = \frac{e^{-jkr}}{4\pi r} \tag{11.106}$$

and the distance r is given by (11.103). The integral equation is obtained by equating this electric field to the negative of electric field produced by the excitation current,

$$\frac{1}{j\omega\epsilon_0} \int_{-\ell/2}^{\ell/2} \left[\frac{\partial^2 G(z; z')}{\partial z^2} + k^2 G(z; z') \right] I(z')\, dz' = -E_z^i \qquad \text{at } \rho = a \tag{11.107}$$

This equation is the electric field integral equation (EFIE) for wire antenna and is also called *Pocklington integro-differential equation*. For a very thin wire, the equation may be simplified as [6]

$$\int_{-\ell/2}^{\ell/2} I(z') \frac{e^{-jkr}}{4\pi r^5} [(1 + jkr)(2r^2 - 3a^2) + (kar)^2]\, dz' = -j\omega\epsilon_0 E_z^i \qquad \text{at } \rho = a \tag{11.108}$$

Next we model the excitation field E_z^i on the wire surface.

Gap Generator Model for the Excitation Field, E_z^i

The impressed/excitation field E_z^i at the surface of wire antenna can be simply modeled by a gap voltage generator as shown in Figure 11.9(a). Here, it is assumed that the excitation of the antenna is due to the applied voltage V_i at the feed gap and zero elsewhere. Therefore, the incident electric field is simply given by

$$E_z^i = \begin{cases} V_i/\Delta & \text{over the feed gap } \Delta \\ 0 & \text{elsewhere} \end{cases} \tag{11.109}$$

This model is the simplest but least accurate for input impedance calculations. The accuracy of the model increases with the decrease in gap width Δ.

Frill Magnetic Current Model for Excitation Field. The feed model based on magnetic frill generator is more accurate [5]. In this model, the excitation is modeled like the coaxial line excitation of a monopole antenna through the ground plane and shown in Figure 11.9(b). The ratio b/a of the coaxial line is designed to produce 50-ohm impedance of coaxial line, and is 2.301 for an air-filled line. The radial electric field in a coaxial line is given by

$$E_f = \hat{\rho}\,\frac{1}{2\rho'}\,\frac{V_i}{\ln\left(\dfrac{b}{a}\right)} \qquad a \le \rho' \le b \tag{11.110}$$

For modeling the excitation field, the coaxial aperture is closed off with a perfect conductor using the equivalence principle (Section 1.7), and an equivalent magnetic frill azimuthal current $-\hat{\phi}2E_f$ is placed in the region $a \le \rho' \le b$. The frill or annular current at the feed location is shown in Figure 11.9(c). The magnetic current produces the following approximate field at the axis of the wire [5, 7]:

$$E_z^i = -\frac{V_i}{2\,\ln\left(\dfrac{b}{a}\right)}\left[\frac{e^{-jkR_1}}{R_1} - \frac{e^{-jkR_2}}{R_2}\right] \tag{11.111}$$

where

$$R_1 = \sqrt{z^2 + a^2}, \qquad R_2 = \sqrt{z^2 + b^2} \tag{11.112}$$

MoM Solution. For conciseness let us write the integral equation of (11.108) in the following form:

$$\int_{-\ell/2}^{\ell/2} I(z')K(z;\,z')\,dz' = -j\omega\epsilon_0 E_z^i \qquad \text{at } \rho = a \tag{11.113}$$

where

$$K(z;\,z') = \frac{e^{-jkr}}{4\pi r^5}\left[(1 + jkr)(2r^2 - 3a^2) + (kar)^2\right] \tag{11.114}$$

We shall use pulse expansion for the current $I(z')$ and point matching at the mid-points of segments z_m as described earlier. The integral equation (11.113) therefore reduces to

$$\sum_{n=1}^{N} \alpha_n \int_{\Delta z_n} K(z_m,\,z')\,dz' \approx -j\omega\epsilon_0 E_z^i(z_m) \qquad m = 1,\,2,\,\ldots\,N \tag{11.115}$$

where Δz_n denotes the nth segment of the wire. Let us denote

$$I_{mn} = \frac{1}{j\omega\epsilon_0} \int_{\Delta z_n} K(z_m, z')\, dz' \tag{11.116}$$

$$= \frac{1}{j\omega\epsilon_0} \frac{1}{4\pi} \int_{z_n - \Delta z/2}^{z_n + \Delta z/2} \frac{e^{-jkr}}{r^5} [(1 + jkr)(2r^2 - 3a^2) + (kar)^2]\, dz'$$

where

$$r = \sqrt{a^2 + (z_m - z')^2} \tag{11.117}$$

Equation (11.115) can therefore be written as

$$\sum_{n=1}^{N} \alpha_n I_{mn} \approx -E_z^i(z_m) \tag{11.118}$$

or

$$\alpha_1 I_{m1} + \alpha_2 I_{m2} + \alpha_3 I_{m3} + \ldots + \alpha_n I_{mn} + \ldots + \alpha_N I_{mN} \approx -E_z^i(z_m) \tag{11.119}$$

The above expression can be interpreted to mean that at $z = z_m$ the sum of the electric field due to all N segments is set equal to the negative of the incident field (to satisfy the boundary condition).

Point matching at N points leads to a set of simultaneous equations in N unknowns, and may be written in the matrix form as

$$[I][\alpha] = \left[-E_z^i\right] \tag{11.120}$$

The matrix equation can be solved for vector $[\alpha]$ by using any standard matrix algorithm. Once we have determined $[\alpha]$, we know the current distribution on the wire, which may be used to calculate the input impedance, radiation pattern, or the radar cross-section of the wire. Next we present results for a half-wave dipole.

Point Matching on a Half-Wave Dipole

A half-wave dipole is expected to be resonant for $\ell = 0.47\lambda$. Let us assume $\lambda = 1$m, and $a = 0.005\lambda$ for the dipole. For convenience we divide the dipole into 11 equal length segments as shown in Figure 11.10. Also, we assume 1 volt excitation at the center of the dipole. The computed electric field and the current obtained using the frill magnetic current model are given in Table 11.2. We note that the current decreases from the center towards the ends as expected.

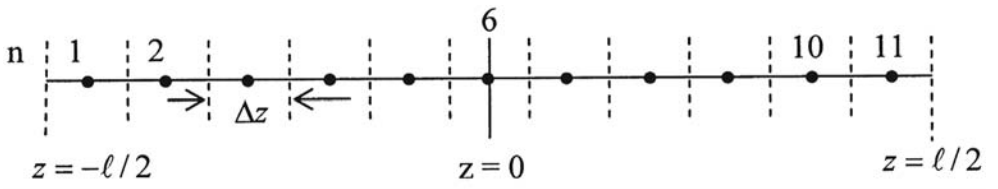

Figure 11.10 A half-wave dipole divided into 11 equal segments of size Δz.

Table 11.2 Computed Electric Field and the Current Vector α for $N = 11$, $b/a = 2.301$, $V_i = 1$ volt

Segment Number, n	*Excitation Vector* $E_z^n, \times 10^{-4}$	*Current Vector* $\alpha, \times 10^{-3}$
1, 11	$-j1$	$9.7 \angle -40$
2, 10	$-j2$	$17 \angle -39$
3, 9	$-j3$	$22.7 \angle -37$
4, 8	$-j10$	$26.5 \angle -35$
5, 7	$-j67$	$28.3 \angle -32$
6	$-j11333$	$27.7 \angle -27$

Input impedance. The input impedance of the dipole can be obtained from the above data. For the feed point located at the center of the dipole, the input impedance is given by

$$Z_{in} = \frac{V_i}{\alpha_6} = \frac{1}{27.7 \times 10^{-3} \angle -27^\circ} = 31.97 + j16.7\Omega \tag{11.121}$$

We observe that the input impedance of a thin dipole of length $0.47\lambda_0$ is inductive. The accurate value of the input impedance for this dipole is $Z_{in} = 80\Omega$.

Effect of Increasing the Number of Segments N. Table 11.3 compares the input impedance for the dipole as a function of the number of segments for the delta-gap and magnetic frill generators. Software *dipole.m* is used for the purpose. The input impedance converges to the true value for $N > 100$ for both the models, but

Table 11.3 Comparison of the Input Impedance of the Half-Wave Dipole for Two Different Source Models ($\ell = 0.47\lambda$, $a = 0.005\lambda$)

Number of Segments, N	*Delta Gap Source*	*Magnetic Frill Source*
11	$94.17 + j49.0$	$31.96 + j16.7$
21	$77.65 - j0.61$	$47.11 - j0.13$
31	$75.15 - j6.6$	$59.52 - j4.6$
51	$77.18 + j2.6$	$73.11 + j4.3$
71	$79.74 + j8.4$	$77.93 + j11.7$
91	$81.43 + j9.16$	$79.52 + j14.68$
111	$82.62 + j7.1$	$80.08 + j15.76$

the behavior of magnetic frill source is regular. Figure 11.11 shows the effect of increasing N on the amplitude of current distribution for the magnetic frill source. The current converges to the expected half-wave sinusoid for $N > 70$. It is observed that delta gap source also produces convergent current distribution but the dipole current increases with the value of N. The input impedance is plotted in Figure 11.12 for a large number of values of N for the magnetic frill source. The real part of input impedance converges to 80 ohms for $N > 80$.

The MoM analysis of wire antenna in terms of Hallen integral equation is described in [8].

11.2.5 Scattering from a Conducting Cylinder of Infinite Length

The scattering of a propagating wave by an object is one of the fundamental phenomena in electromagnetics. The quantity of interest derived from scattering is the radar cross-section (RCS), which is a measure of the effective area of the scatterer, and is a function of both the angle of incidence and the angle of observation. The larger the RCS, the larger is the power scattered by the object. Stealth technologies are used to reduce the RCS so that the object becomes almost invisible to the incident radiation.

The MoM formulation for scattering from an object is very similar to the formulation for antennas. The difference between the two phenomena lies in the

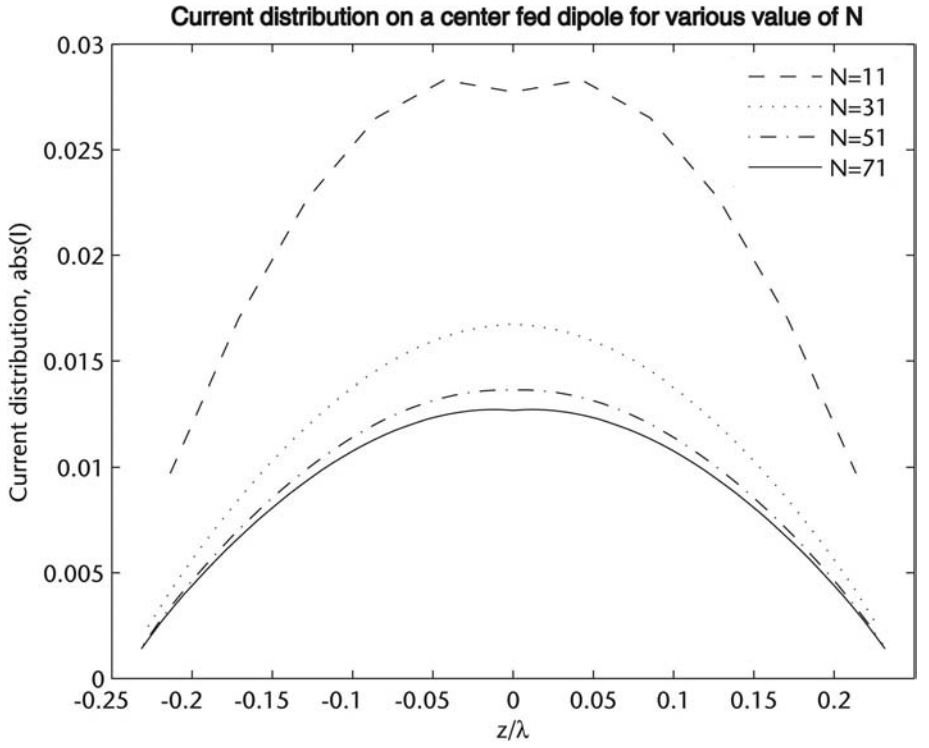

Figure 11.11 Convergence of current distribution on a half-wave wire dipole as a function of N, the number of segments. $\ell = 0.47\lambda$, $a = 0.005\lambda$, $\lambda = 1$m.

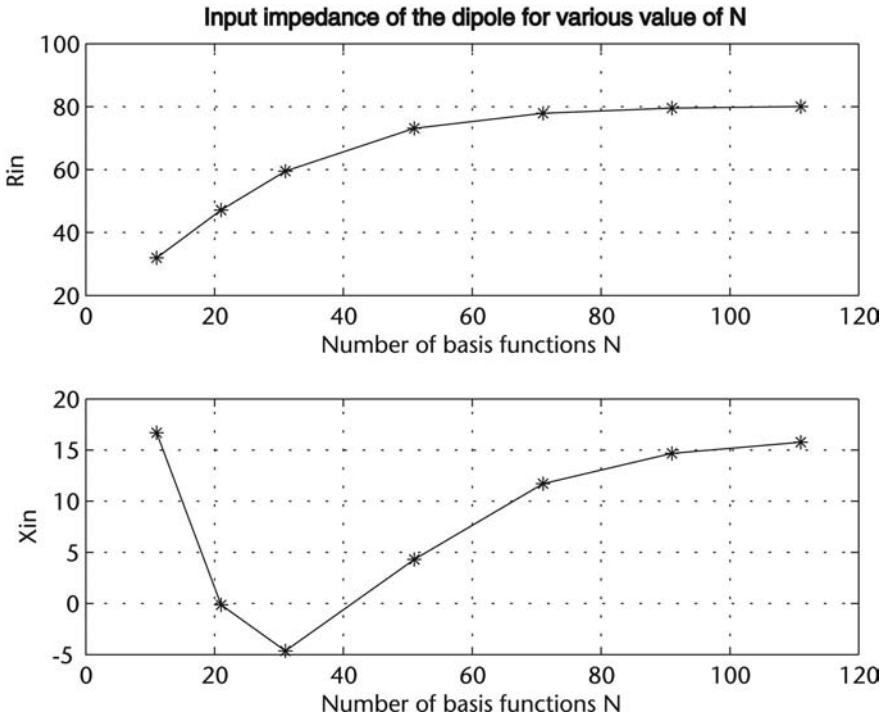

Figure 11.12 Variation of input impedance of wire dipole antenna with pulse basis functions. $\ell = 0.47\lambda$, $a = 0.005\lambda$, $\lambda = 1$m.

source of excitation. In case of antennas, the exciting source is located at the antenna, whereas the exciting source is located at infinity for the purpose of scattering. We shall analyze the problem of scattering by an infinite conducting cylinder. Since there is no reflected wave from the ends of an infinitely long object, the current does not vary along the length, and the problem therefore becomes two dimensional.

An infinitely long, perfectly conducting cylinder is shown in Figure 11.13(a), where the contour C defines the shape of the cylinder. Although the cylinder drawn there is a circular cylinder, the formulation presented next is applicable for cylinders of arbitrary cross-section. The integral equation for the cylinder is obtained by applying the boundary condition that the (total) tangential electric field on its surface is zero; the total electric field consists of the incident field and the scattered field produced by the current induced on the conductor; that is,

$$E_{\tan}^{inc} + E_{\tan}^{scat} = 0 \qquad \text{on the conductor surface} \tag{11.122}$$

Since the source of incident wave is located at infinity, the incident wave is a plane wave over the cross-section of the cylinder. Let us assume the incident wave to be a plane TM wave with $H_z = 0$ and $\mathbf{E} = \hat{z}E_z(x, y)$. The induced current and the scattered field produced by it are related by the vector wave equation (1.28), which becomes the scalar wave equation in this case,

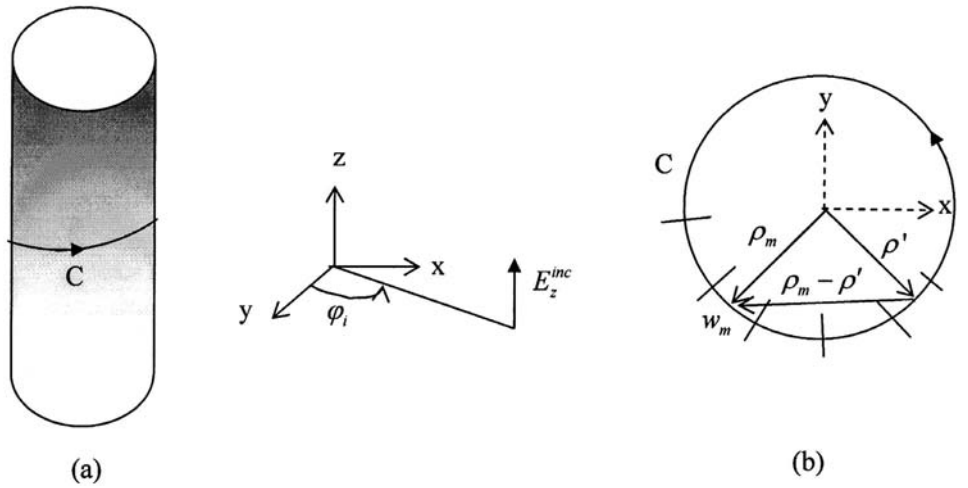

Figure 11.13 (a) TM wave incident on an infinitely long conducting cylinder. (b) Partitioning of contour C and illustration of geometrical parameters.

$$\nabla^2 E_z^{scat} + k^2 E_z^{scat} = j\omega\mu_0 J_z \tag{11.123}$$

because E_z^{inc} induces J_z only. The Green's function solution for the above wave equation is similar to that given in (3.101), and the scattered field may be expressed as

$$E_z^{scat}(\rho) = -\frac{k\eta_0}{4}\int_C J_z(\rho')H_0^{(2)}\big(k|\rho-\rho'|\big)dl' \tag{11.124}$$

where $\rho = \hat{x}x + \hat{y}y$ is the field point, $\rho' = \hat{x}x' + \hat{y}y'$ is the source point on the contour of cylinder, $H_0^{(2)}(.)$ is the Hankel function of second kind and zero order, $\eta_0 \approx 377\Omega$ is the free space impedance, and $k = 2\pi/\lambda$. The Hankel function of second kind is used here, and not first order, because the scattered wave is traveling outward. The integration is carried out over the contour of the cylinder because the current inside a perfect conductor is zero.

Applying the boundary condition (11.122) on contour C gives the integral equation as

$$E_z^{inc}(\rho) = \frac{k\eta_0}{4}\int_C J_z(\rho')H_0^{(2)}\big(k|\rho-\rho'|\big)dl' \tag{11.125}$$

The unknown surface current can now be determined using MoM. The incident plane wave field is assumed to be propagating normal to the z-axis, the axis of the cylinder. Therefore, $\mathbf{k} = \hat{x}k_x + \hat{y}k_y$ and the incident field may be specified as

$$E_z^{inc} = E_0 e^{-j\mathbf{k}.\mathbf{r}} = E_0 e^{-jk(x\cos\varphi_i + y\sin\varphi_i)} \tag{11.126}$$

where φ_i is the angle of incidence as shown in Figure 11.13(a). The analysis next follows the discussion given in [2, p. 38].

For the MoM solution we now divide the contour into a number of segments as shown in Figure 11.13(b) and use pulse expansion for the unknown current as,

$$J_z(\rho') \simeq \sum_{m=1}^{M} \alpha_n P(\rho' - \rho_m) \tag{11.127}$$

where $P(\rho - \rho_m)$ is the pulse function centered at ρ_m. If we divide the contour in sufficiently large number of segments, the curved segment may be replaced by a flat segment. Point matching at the mid-point ρ_n of segments reduces the integral equation (11.125) to

$$E_z^{inc}(\rho_n) = \frac{k\eta_0}{4} \sum_{m=1}^{M} \alpha_m \int_{w_m} H_0^{(2)}\left(k|\rho_n - \rho'|\right) dl' \qquad n = 1, 2, 3, \ldots N \tag{11.128}$$

where w_m is the size of the mth segment. The expression (11.128) can be written as a set of simultaneous equations as ($M = N$)

$$\begin{bmatrix} E_z^{inc}(\rho_1) \\ E_z^{inc}(\rho_2) \\ \vdots \\ E_z^{inc}(\rho_N) \end{bmatrix} = \begin{bmatrix} Z_{11} & Z_{12} & \ldots & Z_{1N} \\ Z_{21} & Z_{22} & \ldots & Z_{1N} \\ \vdots & \vdots & \vdots & \vdots \\ Z_{N1} & Z_{N2} & \ldots & Z_{NN} \end{bmatrix} \begin{bmatrix} \alpha_1 \\ \alpha_2 \\ \vdots \\ \alpha_N \end{bmatrix} \tag{11.129}$$

or in matrix form as

$$[E^{inc}] = [Z][\alpha] \tag{11.130}$$

where

$$Z_{mn} \simeq \frac{k\eta_0}{4} \int_{\rho_m - w_m/2}^{\rho_m + w_m/2} H_0^{(2)}\left(k|\rho_n - \rho'|\right) dl' \tag{11.131}$$

Analytical Simplification of Matrix Elements

The matrix elements are now simplified analytically so that they can be expressed in accurate but simpler form. The diagonal elements are relatively large and contribute significantly to the solution. For segment size small enough compared to the wavelength, (11.131) may be approximated as [1, p. 43]

$$Z_{mn} \simeq \frac{k\eta_0}{4} w_n H_0^{(2)}(kR_{mn}) \qquad \text{for } m \neq n \tag{11.132}$$

and

$$R_{mn} = |\rho_n - \rho_m| = \sqrt{(x_m - x_n)^2 + (y_m - y_n)^2}$$

This approximation is found to be accurate to about 2% when the segment size is about $\lambda/10$ [2].

For diagonal and near-diagonal matrix elements, the argument of the Hankel function is small; and the Hankel function may be expressed as [2, p. 39]

$$H_0^{(2)}(t) \approx \left(1 - \frac{t^2}{4}\right) - j\left\{\frac{2}{\pi}\ln\left(\frac{\gamma t}{2}\right) + \left[\frac{1}{2\pi} - \frac{1}{2\pi}\ln\left(\frac{\gamma t}{2}\right)\right]t^2\right\} + O(t^4) \tag{11.133}$$

where $\gamma = 1.78107\ldots$. Retaining the dominant terms of (11.133), the integration in (11.131) may be carried out as [2, p. 40]

$$\int_{w_m} H_0^{(2)}\left(k|\rho_m - \rho'|\right) dl' \simeq 2 \int_0^{w_m/2} \left[1 - j\frac{2}{\pi}\ln\left(\frac{\gamma k u}{2}\right)\right] du \tag{11.134}$$

$$= w_m - j\frac{2}{\pi} w_m \left[\ln\left(\frac{\gamma k w_m}{4}\right) - 1\right]$$

Using this expression, the diagonal elements are obtained as

$$Z_{mn} \simeq \frac{k\eta_0 w_m}{4}\left\{1 - j\frac{2}{\pi}\left[\ln\left(\frac{\gamma k w_m}{4}\right) - 1\right]\right\} \tag{11.135}$$

A better accuracy in the evaluation of matrix elements can be achieved by numerical integration. For diagonal elements, singularity subtraction may be employed before integration.

The solution of matrix equation (11.130) yields the induced current distribution J_z on the cylinder and is given by

$$[\alpha] = [Z]^{-1}[E^{inc}] \tag{11.136}$$

where $E_m^{inc} = e^{jk(x_m \cos\varphi_i + y_m \sin\varphi_i)}$ and (x_m, y_m) denotes the coordinates of the mid-point of the segment.

The induced current density may be used to determine the RCS of the scatterer. For a two-dimensional scatterer, RCS is defined as [2, p. 24]

$$\sigma_{TM}(\varphi, \varphi^{inc}) = \lim_{\rho \to \infty} 2\pi\rho \left|\frac{E_z^{scat}}{E_z^{inc}}\right|^2 \tag{11.137}$$

and can be expressed in terms of induced current on a perfectly conducting cylinder as

$$\sigma_{TM}(\varphi, \varphi^{inc}) = \frac{k\eta_0^2}{4}\left|\int_C J_z(x', y')\, e^{jk(x'\cos\varphi + y'\sin\varphi)}\, dl'\right|^2 \tag{11.138}$$

For small sized segments, the integral may be approximated by summation over the segments as,

$$\sigma_{TM}(\varphi, \varphi^{inc}) = \frac{k\eta_0^2}{4}\left|\sum_{n=1}^{N} \alpha_n w_n e^{jk(x_n\cos\varphi + y_n\sin\varphi)}\right|^2 \tag{11.139}$$

where φ is the angle of observation. In matrix form, (11.139) may be written as [1, p. 45]

$$\sigma_{TM}(\varphi, \varphi^{inc}) = \frac{k\eta_0^2}{4}\,|\,[V^s][ZS]^{-1}[V^{inc}]\,|^2 \tag{11.140}$$

where $[V^{inc}]$ is an excitation voltage vector, $[V^s]$ is a voltage matrix at the observation angle, and $[ZS]$ is the scatterer impedance matrix, defined as

$$V_m^{inc} = w_m e^{jk(x_m\cos\varphi_i + y_m\sin\varphi_i)},\ V_n^s = w_n e^{jk(x_n\cos\varphi + y_n\sin\varphi)},\ ZS_{mn} = w_m Z_{mn} \tag{11.141}$$

The above formulation is coded for a circular cylinder of radius a. The software is called *scattering_circular.m*. The plane TM wave is defined by $E_z^{inc} = e^{-jk(x\cos\varphi_i + y\sin\varphi_i)}$ and $\varphi_i = \pi$. The computed induced current on the surface of the cylinder is plotted in Figure 11.14 as a function of φ for two values of ka. The current is maximum on the illuminated side $\varphi = \pi$ of the cylinder and becomes almost negligible in the shadow region. Also, the induced current increases with the increase in the value of ka.

It has been observed that for best accuracy of the above scatterer model, the phase center (x_m, y_m) of each segment should be located on the surface of the original cylinder and the segment width is obtained from the circumference of the original cylinder [2] as $w_m = 2\pi a/N$, where N is the number of segments.

The radar cross-section of the cylinder is computed using (11.140), and the normalized value $\sigma/(2\pi a)$ is plotted in Figure 11.15 as a function of angle of observation φ for $ka = 1$ and 4. The RCS is higher in the direction of shadow region and relatively low on the illuminated side of the cylinder. It is contrary to the distribution of induced current on the cylinder. This paradox is explained by the fact that incident radiation is present for all values of φ, whereas the scattered radiation is more on the illuminated side and cancels the incident radiation there. The scattered field being less on the shadow region, the incident radiation contributes significantly to the RCS in the shadow region [9, p. 129]. Also, the figure

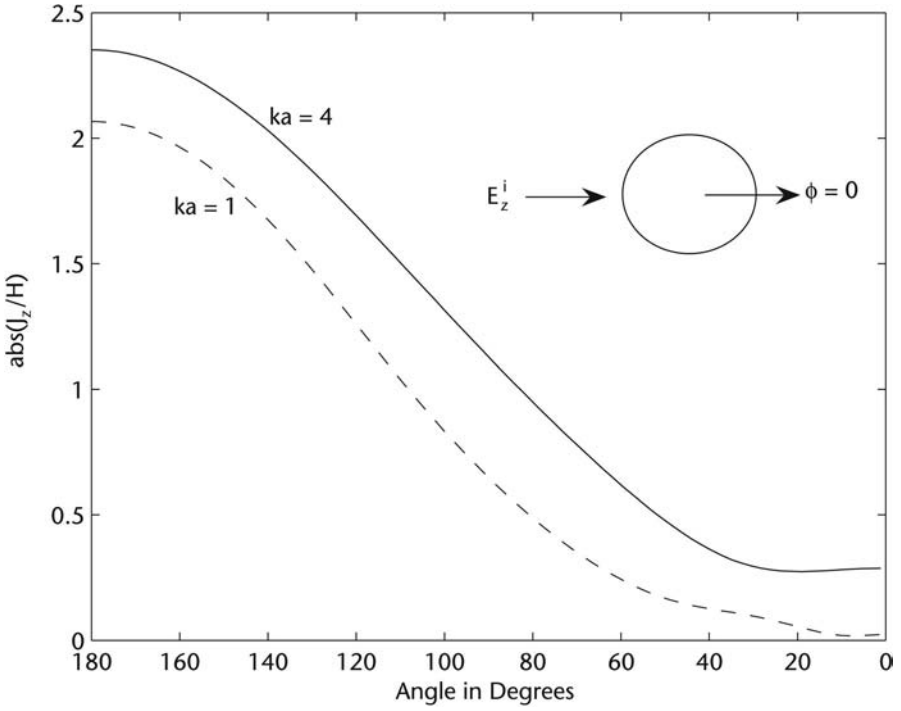

Figure 11.14 Induced current on a conducting circular cylinder of radius $a = 1$m, $N = 160$.

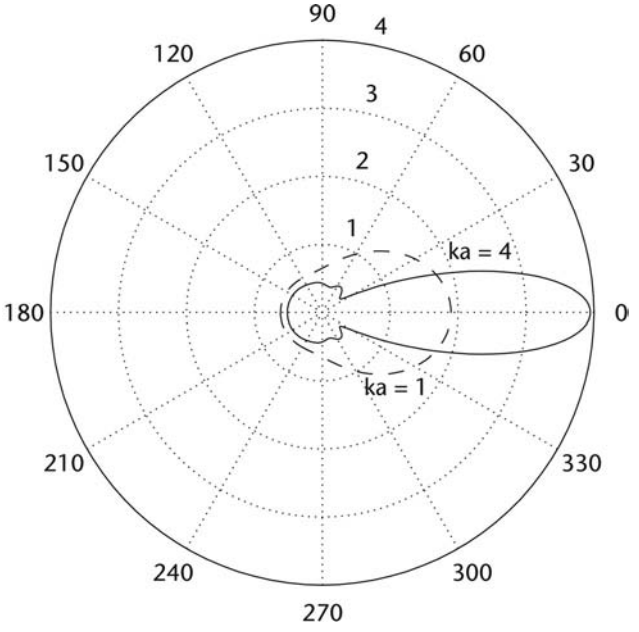

Figure 11.15 RCS ($\sigma/2\pi a$) of a circular cylinder of radius $a = 1$m, $N = 160$.

shows that RCS becomes more directive with the increase in the value of ka. The increase in ka was realized by increasing the frequency of the incident wave and keeping radius a fixed.

Analytical Solution for the Circular Cylinder

The circular cylinder, being a regular shaped geometry, has been analyzed using the method of separation of variables. For this, the incident plane wave is expanded in terms of cylindrical functions as [10, p. 233].

$$E_z^{inc} = E_0 e^{-jk\rho\cos\varphi_i} = E_0 \sum_{n=-\infty}^{\infty} j^{-n} J_n(k\rho) e^{jn\varphi_i} \tag{11.142a}$$

The scattered field is similarly expressed as

$$E_z^{scat}(\rho) = E_0 \sum_{n=-\infty}^{\infty} j^{-n} a_n H_n^{(2)}(k\rho) e^{jn\varphi_i} \tag{11.142b}$$

Applying the boundary condition (11.122) at the surface of the cylinder $\rho = a$ gives the following expression for the expansion coefficients a_n:

$$a_n = -\frac{J_n(ka)}{H_n^{(2)}(ka)} \tag{11.143}$$

The surface current on the cylinder is therefore given by

$$J_z = H_\varphi\big|_{\rho=a} = \frac{1}{j\omega\mu_0}\frac{\partial}{\partial\rho}\left(E_z^{inc} + E_z^{scat}\right)\Big|_{\rho=a} \tag{11.144}$$

Using (11.142) in (11.144) and simplifying the result by means of Wronskian,

$$J_n(x)H_n'^{(2)}(x) - H_n^{(2)}(x)J_n'(x) = \frac{2}{\pi x} \tag{11.145}$$

yields

$$J_z = -\frac{2E_0}{\omega\mu_0\pi a}\sum_{n=-\infty}^{\infty}\frac{j^{-n}e^{jn\varphi_i}}{H_n^{(2)}(ka)} \tag{11.146}$$

The scattered electric field at large distances from the cylinder may be obtained from (11.142b) by using the following asymptotic formula for $H_n^{(2)}(k\rho)$:

$$H_n^{(2)}(x) \xrightarrow[x\to\infty]{} \sqrt{\frac{2j}{\pi x}}\, j^n e^{-jx} \tag{11.147}$$

The scattered field is therefore obtained as

$$E_z^{scat} \xrightarrow[k\rho\to\infty]{} E_0\sqrt{\frac{2j}{\pi k\rho}}\,e^{-jk\rho}\sum_{n=-\infty}^{\infty} a_n e^{jn\varphi_i} \tag{11.148}$$

The ratio of the scattered field to the incident field is given by

$$\left|\frac{E_z^{scat}}{E_z^{inc}}\right|^2 = \sqrt{\frac{2}{\pi k\rho}}\left|\sum_{n=-\infty}^{\infty}\frac{J_n(ka)}{H_n^{(2)}(ka)}e^{jn\varphi_i}\right| \tag{11.149}$$

The convergence of this series is slow for large values of ka; for example, six terms give satisfactory result for $ka = 3$, whereas 100 terms are needed for $ka = 100$.

RCS of a Square Cylinder

Next, we study the scattering by a square cylinder to observe the role played by the corners/wedges on the scatterer. The formulation described earlier was coded for a square cylinder of side length $a = 1$m and $ka = 1, 4$. The software is called *scattering_square.m*. The induced current on the cylinder is plotted in Figure 11.16. Due to the symmetry of the cylinder and excitation, the current distribution on only half the cross-section is plotted. The current is found to be singular at the corner facing the incident wave. The current decreases almost linearly towards the shadow region, except at the corner in that region. Also, the induced current increases with ka. The normalized RCS $\sigma/(4a)$ was computed for the square cylinder and is plotted in Figure 11.17. Comparing this plot with Figure 11.15 for the RCS

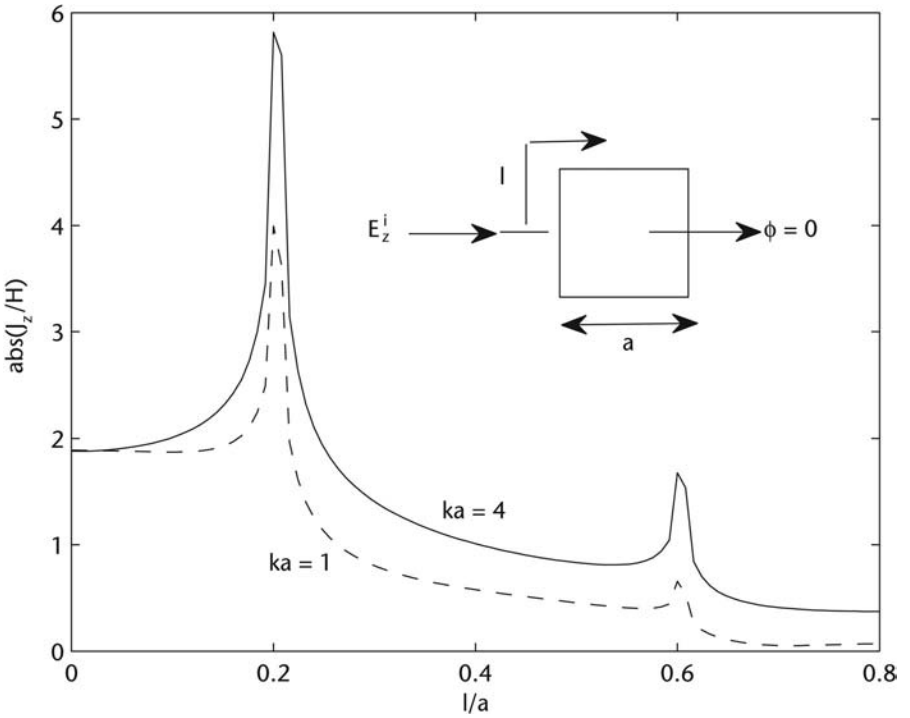

Figure 11.16 Induced current on a square cylinder of side a. $N = 200$.

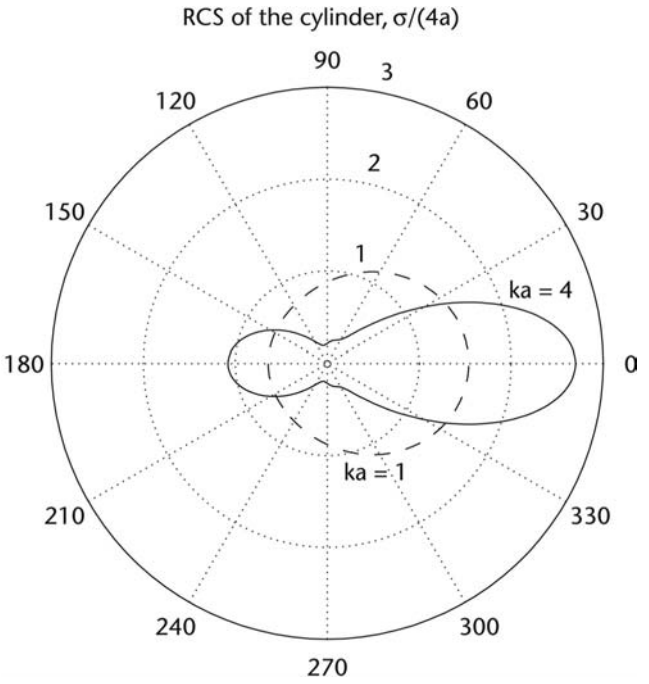

Figure 11.17 RCS ($\sigma/(4a)$) of a square cylinder of side a. $N = 200$.

of a circular cylinder, we find that the RCS of a square cylinder is less directive although the induced current is highly peaked.

11.3 Fast Multipole Solution Methods for MoM

The MoM is an efficient method with less number of unknowns. However, the matrix is dense and the use of direct solution methods, such as LU decomposition, results in large number of floating point operations, which increase with frequency as $O(f^6)$. The processor time can be reduced by using Fourier transformation or CG-FFT techniques for geometries that are thin along one direction [11]. For truly three-dimensional geometries, several methods have been proposed for efficient MoM solution. A very successful scheme involves replacing the matrix-vector multiplication of MoM by the fast multipole method (FMM) and its variant multilevel fast multipole [12]. The first step in this method is to divide the simulation region into a number of subregions, each containing a number of cells. Computations for the cells in the same or adjacent subregions are carried out in the standard way as described earlier. However, the fields produced by the sources far away from the observation cell are computed by multipole expansion of the sources and then projecting this onto a set of plane waves in the observation cell. The efficiency is achieved because only a few terms of the multipole expansion are needed. The number of floating point operations based on FMM increases as $O(f^3)$ and can be reduced to $O(f^2 \log f)$ if the multilevel extension of FMM is implemented. In the multilevel FMM, the FMM algorithm is repeated in a hierarchical fashion

similar to that in a telephone network. In a network of N customers, a number of N^2 connections is required if a direct line connects every other customer. The number of connections can be reduced by introducing hubs. To make a telephone call, a customer calls the local hub, which calls another hub, and finally to the recipient of the call.

11.4 Comparison of FDM, FDTD, FEM, and MoM

We have discussed a number of computational methods to solve problems with simple geometries and dielectric inhomogeneities. A common base for FDM, FEM, and MoM is the weighted residual method [13]. The common features of these methods include discretization of the unknown function, approximations, and the solution based on matrix solution techniques. The approximations result in inaccuracies. The convergence and spurious solutions are other problems. We compare the computational methods with these perspectives in Table 11.4. The evaluation is not quantitative but qualitative. With the limited experience we have developed with the computational methods in terms of rectangular grid and one-dimensional and two-dimensional geometries, we can compare the methods in a limited manner only.

Table 11.4 Qualitative Comparison of Computational Methods

Characteristics	*FDM*	*FDTD*	*FEM*	*MoM*
Preprocessing	Nil	Nil	Moderate	Significant (because of Green's function)
Level of discretization	Surface level	Surface level	Surface level	Contour level
Stability of solution	Good	Poor, if not causal	Good	Very good
Matrix type	Sparse	—	Sparse	Dense
Storage requirement	Large	Very Large	Large	Small to moderate
CPU time	Large	Large	Moderate to large	Small to moderate
Numerical dispersion	Yes	Yes	Yes	No
Analysis of arbitrary shaped geometry	Poor, if rectangular or cylindrical mesh is used	Poor, if rectangular or cylindrical mesh is used	Very good, if triangular elements are employed	Good (only the unknown function is discretized)
Open boundary problems	Convergence is very slow if first order ABC is used	PML or ABC may be used to truncate the domain	PML or ABC may be used to truncate the domain	Efficient (because of Green's function)
Spurious solutions	No	No	Yes, for node based elements	No
Distinctive feature	Easier to understand, but inefficient	Versatile, can produce animation	Analysis of arbitrary shaped geometry	Efficient for open boundary problems.

The various aspects of the computational methods dealt with in this text should be useful in developing the necessary skills. An experienced student can accelerate numerical processing skillfully.

11.5 Hybrid Computational Methods

As discussed in the last section, the computational methods in their classical form suffer from one limitation or the other. MoM results in a dense matrix although the number of unknowns is less, whereas FEM suffers from large number of unknowns. For the unbounded region problems, MoM has the advantage associated with the use of Green's function, whereas FEM is versatile for inhomogeneous medium problems. It is possible to combine the useful features of FEM and MoM so that unbounded region problems with inhomogeneous dielectric could be solved efficiently. The resulting hybrid method is called finite element-boundary integral (FE-BI) method. The formulation of FE-BI by Botha and Jin [14] is based on variational formulation and is very well described in [15, Ch.10]. FEM has been combined with conformal mapping to determine the capacitance of printed lines [16]. Computational efficiency of FDTD may be combined with the body conforming meshing property of FEM [17].

11.6 Summary

The method of moments (MoM) is a powerful computational method which is partly analytical and partly computational. The method is very efficient for the analysis of open region geometries such as antennas, scatterers, and planar circuits. The method is based on weighted residual method in which the residue of the governing equation is set to zero in an average sense over the domain. The unknown function is expanded in a set of expansion functions, and inner product of the residue is set to zero. The number of test functions are taken equal to the number of expansion functions in order to generate as many equations as there are unknowns. The MoM is illustrated by solving a number of examples like, strip line capacitance, charge distribution on a metal wire, current distribution and input impedance of a half-wave dipole, and RCS of a cylindrical scatterer. Various computational methods discussed in the book are compared

References

[1] Harrington, R. F., *Field Computation by Moment Methods*, Malabar, FL: R.E. Kreiger Publishing Co., 1982.

[2] Peterson, A. F., S. L. Ray, and R. Mittra, *Computational Methods for Electromagnetics*, New York: IEEE Press, 2001.

[3] Neff, H. P., Jr., *Basic Electromagnetic Fields*, 2nd ed., New York: Harper & Row, 1987.

[4] Wilton, D. R., and S. Govind, "Incorporation of Edge Condition in the Moment Method Solutions," *IEEE Trans. Antennas Propagat.*, Vol. AP-25, 1977, pp. 845–850.

[5] Balanis, C. A., *Antenna Theory: Analysis and Design*, 2nd ed., New York: John Wiley, 1982.

[6] Stutzman, W. L., and G. A. Thiele, *Antenna Theory and Design*, New York: John Wiley, 1981.

[7] Jordan, E. C., and K. G. Balmain, *Electromagnetic Waves and Radiating Systems*, Englewood Cliffs, NJ: Prentice-Hall, 1968.

[8] Tsai, L. L., and C. E. Smith, "Moment Methods in Electromagnetics for Undergraduates," *IEEE Trans. Edu.*, Vol. E-31, 1978, pp. 14–22.

[9] Moore, J., and R. Pizer, (eds.), *Moment Methods in Electromagnetics: Techniques and Applications*, New York: Research Studies Press, 1984.

[10] Harrington, R. F., *Time Harmonic Electromagnetic Fields*, New York: McGraw-Hill, 1961.

[11] Peters, T. J., and J. L. Volakis, "Application of a Conjugate Gradient FFT Method to Scattering from Thin Material Plates," *IEEE Trans. Antennas Propagat.*, Vol. 36, 1988, pp. 518–526.

[12] Chew, W. C., et al., *Fast and Efficient Algorithms in Computational Electromagnetics*, Norwood, MA: Artech House, 2001.

[13] Sadiku, M. N. O., and A. F. Peterson, "A Comparison of Numerical Methods for Computing Electromagnetic Eields," *Proc. 1990 Southeastcon*, pp. 42–47.

[14] Botha, M. M., and J. M. Jin, "On the Variational Formulation of Hybrid Finite Element-Boundary Integral Techniques for Electromagnetic Analysis," *IEEE Trans. Antennas Propagat.*, Vol. 52, 2004, pp. 3037–3047.

[15] Jin, J., *The Finite Element Method in Electromagnetics*, 2nd ed., New York: Wiley, 2002.

[16] Chang, C. N., and J. F. Cheng, "Hybrid Quasistatic Analysis of Multilayer Microstrip Lines," *IEE Proc. H, Microwaves, Antennas and Propagat.*, Vol. 140, April 1993, pp. 79–83.

[17] Rylander, T., and A. Bondeson, "Stability of Explicit-Implicit Hybrid Time-Stepping Schemes for Maxwell's Equations," *J. Comput. Phys.*, Vol. 179, 2002, pp. 426–438.

Problems

P11.1. Solve the following differential equation for the transmission line half-wave resonator using the MoM:

$$\frac{d^2E_y}{dx^2} + \pi^2 E_y(x) = \delta(x - 0.5) \qquad 0 \le x \le 1$$

subject to $E_y(0) = E_y(0) = 0$. Divide the domain into equal segments and use triangular basis and test functions. Obtain the expressions for the matrix element l_{mn} and the excitation vector element p_m.

P11.2. Solve the following ordinary differential equation:

$$-\frac{d^2f}{dx^2} = 1 + x^2 \qquad 0 \le x \le 1$$

subject to $f(0) = f(1) = 0$. Use triangular function expansion-point matching, and Galerkin triangular expansion to determine the function $f(x)$. Comment on the

convergence aspect in the two cases, and determine the residual for triangular function expansion point-matching method.

P11.3. The following problem interprets the finite difference method in the language of MoM [2, p. 228].

1. Use MoM to construct discretization of the following scalar wave equation

$$\frac{d^2E_y}{dx^2} + k^2E_y(x) = g(x) \qquad 0 \le x \le 1$$

using triangular basis functions for E_y. Enforce the differential equation with pulse testing functions such that basis functions straddle two cells of dimension Δx, while the test functions are defined between the centers of adjacent cells as shown in Figure 11.18. Determine the mnth entry of the resulting matrix.

2. Construct a second order finite difference discretization of the wave equation of (1) using cells of dimension Δx and central-difference formula

$$\frac{d^2E_y}{dx^2} = \frac{E_y(i+1) - 2E_y(i) + E_y(i-1)}{(\Delta x)^2}$$

Identify the entries of the tridiagonal finite difference matrix and compare with the entries of the matrix in part (1). Discuss the implications.

P11.4. A parallel strip transmission line consists of two finite width strips running parallel to each other and separated by a distance $2h$, as shown in Figure 11.19. Use the MoM to determine (and plot) the charge density distribution on any of the strips and the characteristic impedance Z_0 of the line for $w = 5$m and $h = 1$m. You may use pulse expansion and point matching with $N = M = 3, 7, 11, 18, 39, 59$, where N and M represent the number of segments on the upper and lower plates, respectively. Also plot Z_0 as a function of w/h for $w/h = 1, 3, 5, 7, 10$ [8].

P11.5. For the center-fed dipole with $\ell = 0.47\lambda$, $a = 0.05\lambda$, and $\lambda = 1$m, determine the input impedance as a function of frequency with frequency ranging from 250 to 350 MHz at an interval of 10 MHz.

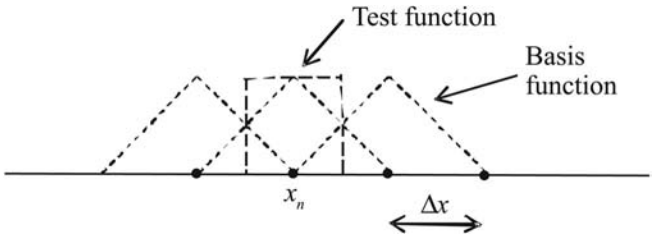

Figure 11.18 Arrangement of triangular and pulse functions to compute matrix element l_{mn}.

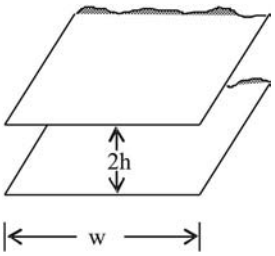

Figure 11.19 Geometry of a parallel strip line.

P11.6. The strip line of Section 11.2 was analyzed using pulse expansion and point matching. Now use triangular expansion and Galerkin's method to determine the expression for matrix elements.

P11.7. Use the expression for matrix elements derived in P11.6 to determine the charge distribution on the strip for the set of parameters considered in Section 11.2. Comment on the convergence behavior.

P11.8. Consider the parallel strip transmission line of Figure 11.19. The MoM analysis of the geometry with pulse expansion and point matching produces the following data for the Z_0 of the line as a function of expansion functions N and w/h:

$N\rightarrow$ $w/h\downarrow$	3	7	11	18	39	59
1	127.72	126.57	126.36	126.27	126.27	126.28
3	69.13	69.30	69.37	69.45	69.57	69.61
5	47.21	48.40	48.69	48.90	49.10	49.17
7	35.19	37.15	37.59	37.89	38.16	38.24
9	27.38	30.03	30.59	30.95	31.27	31.36

1. Determine the most accurate value of Z_0 for each value of w/h. Determine the corresponding capacitance per unit length C.
2. Now model C as a combination of parallel plate capacitance C_p and fringing field capacitance C_f such that $C = C_p + 2C_f$. Determine C_f and plot C_f/C_p as a function of w/h.
3. Explain the behavior of C_f physically.

P11.9. Compare MoM, FDM, and FEM techniques in relation to the solution of

$$-\frac{d^2V}{dx^2} = \pi^2 \sin(\pi x) \qquad 0 \le x \le 1$$

subject to $V(0) = V(1) = 0$.

P11.10. Consider the following one-dimensional scalar Helmholtz equation:

$$\frac{d^2E_y(x)}{dx^2} + k^2E_y(x) = 0, \qquad 0 \le x \le 1$$

where $k = 2\pi/\lambda$ defines the wavelength in the medium.

1. Apply FDM and the central difference approximation to determine the mnth entry of the resulting matrix.
2. Apply MoM and the triangular basis and testing functions of size $2\Delta x$ to determine the mnth entry of the resulting matrix.
3. Apply FEM and the triangular basis and testing functions of size $2\Delta x$ to determine the mnth entry of the resulting matrix.
4. Compare the entries of (1), (2), and (3) and discuss the implications.